THE UNIVERSITY OF MICHIGAN

INDUSTRY PROGRAM OF THE COLLEGE OF ENGINEERING

THERMAL STRESSES IN THICK-WALLED TUBES WITH LAMINAR CONVECTION HEAT TRANSFER

Daniel P. Werner

A dissertation submitted in partial fulfillment
of the requirements for the degree of
Doctor of Philosophy in
The University of Michigan

April, 1968

IP-818

ACKNOWLEDGMENTS

I am sincerely grateful to Professor V. S. Arpaci, Chairman of the doctoral committee, for his patience, invaluable suggestions, and personal interest during this investigation. I also wish to thank the remaining members of my doctoral committee for their advice and suggestions.

The financial support of the experimental work by the Shell Oil Company is gratefully acknowledged, as is the financial support provided by the Department of Mechanical Engineering and the Horace H. Rackham School of Graduate Studies, University of Michigan.

Finally, I wish to thank my wife for her patience, encouragement, and sacrifices.

TABLE OF CONTENTS

LIST OF FIGURES

LIST OF FIGURES (Continued)

NOMENCLATURE

A_m	coefficients for modified Graetz solution
a	Helmholtz function
B	modified Biot number
B_m	coefficients for modified Graetz solution
$\overline{B}$	parameter including modified Biot number
C	constant deformation specific heat
C	constant in modified Leveque solution
C_f	constant pressure specific heat of fluid
E	modulus of elasticity
e	cubical dilitation
G	shear modulus
h	heat transfer coefficient
$\overline{h}$	overall heat transfer coefficient
I_ν	modified Bessel function of first kind of order ν
J_ν	Bessel function of first kind of order ν
K_ν	modified Bessel function of second kind of order ν
k, k_f	thermal conductivity of solid and fluid, respectively
M_m	coefficients in particular stress solution
N	modified Nusselt modulus
m	integer
Pe	Peclet number
q_r, q_z	radial and axial heat flux, respectively
R	dimensionless radial coordinate
R_o	dimensionless outside radius

R	radial body force
R_m	eigenfunction
r	radial coordinate
r_i	inside radius
r_o	outside radius
S	Laplace transform parameter
s	entropy
T	tube-wall temperature
T_f	fluid temperature
T_o	inlet temperature
T_∞	ambient temperature
t	time
U	average velocity
u	radial displacement
u_c, u_p	complimentary and particular solution for u, respectively
$\bar{u}$	internal energy
u^*	local fluid velocity
$\vec{V}$	displacement vector
w	axial displacement
w_c, w_p	complimentary and particular solution for w, respectively
Y_ν	Bessel function of second kind of order ν
y	transverse coordinate
Z	dimensionless axial coordinate
$\bar{Z}$	dimensionless axial coordinate
Z_z	axial body force
z	axial coordinate

β	thermal coefficient of expansion
Γ	Gamma function
Δ	percentage deviation in temperature
γ	shear strain
γ	arbitrary end parameter
$\epsilon_r, \epsilon_z, \epsilon_\varphi$	radial, axial, and tangential strain components
ζ	axial coordinate
η	transverse coordinate
θ	dimensionless fluid temperature
θ_1, θ_2	dimensionless temperature
θ_1^*, θ_2^*	dimensionless temperature
θ	dimensionless fluid temperature
$\bar{\theta}$	transformed dimensionless fluid temperature
θ^*	dimensionless fluid temperature
Λ	Boussinesq-Papkovich displacement potential
λ	separation parameter
λ_m	eigenvalue
μ_m	eigenvalue parameter
ν	Poisson's ratio
ξ	transverse coordinate
ρ, ρ_f	density of solid and fluid, respectively
$\sigma_r, \sigma_z, \sigma_\varphi$	radial, axial, and tangential stress components, respectively
$\sigma_r^*, \sigma_z^*, \sigma_\varphi^*$	dimensionless radial, axial, and tangential stress components, respectively
τ	shear stress
τ^*	dimensionless shear stress

ϕ	dimensionless tube-wall temperature
χ	Love-Galerkin displacement potential
ψ	Goodier displacement potential

CHAPTER I

INTRODUCTION

The basic equations of heat conduction and thermoelasticity are well known and have been in existence for a long time. However, the number of existing three-dimensional solutions appearing in the literature is very small and most of these have been published recently. Comprehensive bibliographies have appeared recently in the texts by Nowacki,[11] Parkus,[13] and Boley and Weiner.[3]

Many of the three-dimensional solutions deal with the axisymmetric distribution of stress in cylinders. Two of major interest are mentioned here. Youngdahl and Sternberg[18] obtained an exact quasi-static solution for the thermal stresses which arise in an infinitely long elastic circular shaft when its surface temperature undergoes a step-change over a finite band. The surface temperature over the remaining portion of the cylinder was held constant. The thermal stresses in pipes were investigated by Parkus.[14] The case of a hot liquid in steady flow through a long tube transferring heat to the surroundings was considered. The inside and outside heat transfer coefficient was assumed to be large and slug flow was assumed to exist in the pipe. It was pointed out in these investigations that the assumption of infinite heat transfer coefficient is unrealistic but will lead to a conservative estimate of the stresses in an actual situation. However, it is often important that more realistic values be obtained since in many practical cases the conservative result greatly overestimates the actual stresses. It is therefore desirable that more realistic physics be included in the formulation of the problem.

It is the purpose of the present investigation to consider a more physically meaningful model to Parkus' problem. The thermal part of the study is based on a modification of the classical Graetz problem in convection heat transfer by including the heat capacity of the tube wall. (For a review of earlier work on the Graetz problem see for instance, Knudsen and Katz[8] or Jakob[7]). It is assumed that heat is transferred to the ambient through an overall heat transfer coefficient which includes both the thermal resistance of the wall and the convective film coefficient.

The modified Graetz problem described above was studied by Schenk and Dumore.[15] Use of the separation of variables led to an eigenvalue problem of the Sturm-Liouville type. Numerical results were given for three values of the finite overall heat transfer coefficient and the first three terms of the series solution were given.

The results of Schenk and Dumore are extended to include six values of the overall heat transfer coefficient. In addition the series solution is extended to practical limits using numerical computation procedures. Since the series solution near the entrance is slowly convergent an approximation based on a modification of the classical Levenque problem (see for instance, Knudsen and Katz[8]) and valid in a small region near the entrance is obtained.

For the thermal stresses associated with the problem it is common practice to estimate these stresses by the plane strain approximation. In this study the exact axisymmetric stress state is determined and the validity of using the plane strain approximation is investigated.

The general thermoelastic formulation for the axisymmetric distribution of stress in cylindrical coordinates is derived from basic principles. The approach used gives physical significance to the various terms in the formulation. For steady problems the formulation reduces to the uncoupled quasistatic theory.

The thermal stresses are found in terms of Goodier and Love-Galerkin displacement potentials. On the cylindrical surfaces the boundary conditions are satisfied exactly while at the entrance the stresses are self-equilibriating and Saint Venant's principle applies.

Representative numerical results are given for surface temperature and stress. Experimental verification of the analytical results was obtained and a limited amount of data is presented.

CHAPTER II

THEORETICAL ANALYSIS

A. Formulation

1. Thermoelastic Formulation of Axisymmetric Problem

The general axisymmetric problem is considered. The equations of motion and thermodynamics are applied to a system. Then the compatibility and constitutive relations are introduced. Finally the steady thermoelastic formulation is obtained.

Application of Newton's second law of motion to the system shown in Figure 1 yields

$$\frac{1}{r}\frac{\partial}{\partial r}(r\sigma_r) + \frac{\partial \tau}{\partial z} - \frac{\sigma_\theta}{r} + R = \rho \frac{\partial^2 u}{\partial t^2} \qquad (1)$$

$$\frac{\partial \sigma_z}{\partial z} + \frac{1}{r}\frac{\partial}{\partial r}(r\tau) + Z = \rho \frac{\partial^2 w}{\partial t^2} \qquad (2)$$

where σ_r denotes the radial stress, σ_z the axial stress, σ_θ the tangential stress, τ the r-z shear stress, r the radial coordinate, z the axial coordinate, t the time, R and Z the radial and axial body forces per unit volume, respectively, ρ the mass density, u the radial displacement, and w the axial displacement. It is noted that since no circumferential distortion occurs the r-θ and θ-z shear stresses are zero. Furthermore, moment of momentum requires that $\tau_{rz} = \tau_{zr} = \tau$.

Applying the first law of thermodynamics to the system yields

$$\rho \frac{\partial \bar{u}}{\partial t} + \frac{1}{2}\rho \frac{\partial}{\partial t}\left(\frac{\partial u}{\partial t}\right)^2 + \frac{1}{2}\rho \frac{\partial}{\partial t}\left(\frac{\partial w}{\partial t}\right)^2 = -\frac{1}{r}\frac{\partial}{\partial r}(rq_r) - \frac{\partial q_z}{\partial z}$$

$$+ \frac{\partial}{\partial z}\left(\sigma_z \frac{\partial w}{\partial t}\right) + \frac{1}{r}\frac{\partial}{\partial r}\left(r\tau \frac{\partial w}{\partial t}\right) + \frac{1}{r}\frac{\partial}{\partial r}\left(r\sigma_r \frac{\partial u}{\partial t}\right) + \frac{\partial}{\partial z}\left(\tau \frac{\partial u}{\partial t}\right) + Z\frac{\partial w}{\partial t} + R\frac{\partial u}{\partial t} \qquad (3)$$

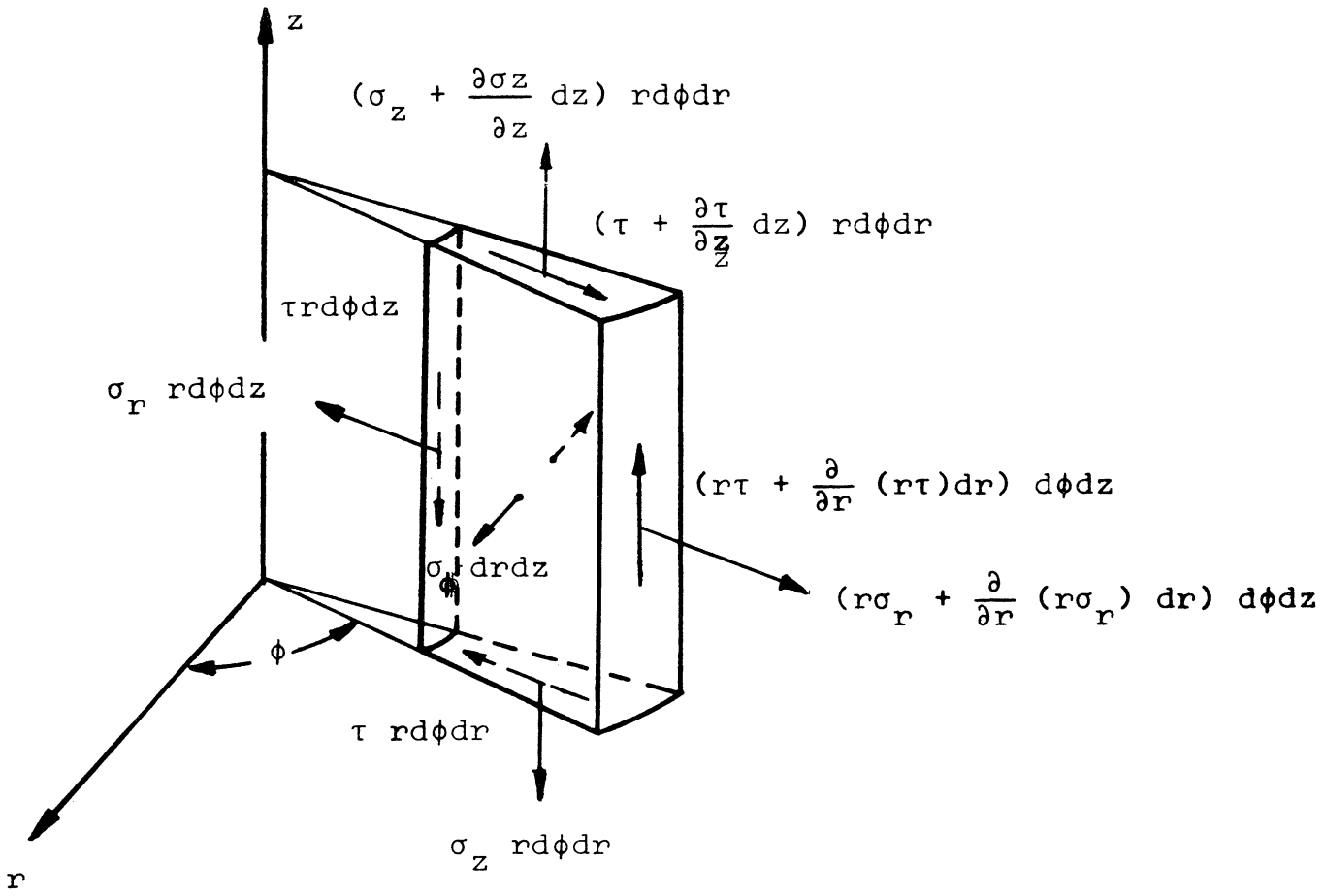

Figure 1. Schematic of System.

where $\bar{u}$ denotes internal energy per unit mass, q_r the radial heat flux, and q_z the axial heat flux.

Multiplication of Equations (1) and (2) by $\frac{\partial u}{\partial t}$ and $\frac{\partial w}{\partial t}$, respectively, yields relations expressing conservation of mechanical energy. Subtraction of these from Equation (3) gives the following expression for the conservation of thermal energy:

$$\rho \frac{\partial \bar{u}}{\partial t} = -\frac{1}{r}\frac{\partial}{\partial r}(r q_r) - \frac{\partial q_z}{\partial z} + \sigma_r \frac{\partial^2 u}{\partial r \partial t} + \frac{\sigma_\varphi}{r}\frac{\partial u}{\partial t}$$

$$+ \sigma_z \frac{\partial^2 w}{\partial z \partial t} + \tau \frac{\partial^2 w}{\partial r \partial t} + \tau \frac{\partial^2 u}{\partial z \partial t} \qquad (4)$$

Here the internal energy may be expressed as a function of temperature by considering

$$\bar{u} = \bar{u}(T, \epsilon_r, \epsilon_\varphi, \epsilon_z, \gamma)$$

where T denotes temperature, ϵ_r the radial strain, ϵ_φ the circumferential strain, ϵ_z the axial strain, and γ the $r-z$ shear strain. The total differential of $\bar{u}$ is

$$d\bar{u} = \left(\frac{\partial \bar{u}}{\partial T}\right)_{\epsilon_r, \epsilon_\varphi, \epsilon_z, \gamma} dT + \left(\frac{\partial \bar{u}}{\partial \epsilon_r}\right)_{T, \epsilon_\varphi, \epsilon_z, \gamma} d\epsilon_r$$

$$+ \left(\frac{\partial \bar{u}}{\partial \epsilon_\varphi}\right)_{T, \epsilon_r, \epsilon_z, \gamma} d\epsilon_\varphi + \left(\frac{\partial \bar{u}}{\partial \epsilon_z}\right)_{T, \epsilon_r, \epsilon_\varphi, \gamma} d\epsilon_z + \left(\frac{\partial \bar{u}}{\partial \gamma}\right)_{T, \epsilon_r, \epsilon_\varphi, \epsilon_z} d\gamma \qquad (5)$$

In terms of the thermodynamic property relationship (which is valid both for reversible and irreversible processes)

$$d\bar{u} = T\,ds + \frac{1}{\rho}(\sigma_r\, d\epsilon_r + \sigma_\varphi\, d\epsilon_\varphi + \sigma_z\, d\epsilon_z + \tau\, d\gamma) \qquad (6)$$

where s denotes the entropy per unit mass. Equation (5) may be rearranged to give

$$d\bar{u} = C_{\epsilon_r, \epsilon_\varphi, \epsilon_z, \gamma}\, dT + \left[T\left(\frac{\partial A}{\partial \epsilon_r}\right)_{T, \epsilon_\varphi, \epsilon_z, \gamma} + \frac{1}{\rho}\sigma_r \right] d\epsilon_r$$

$$+ \left[T\left(\frac{\partial A}{\partial \epsilon_\varphi}\right)_{T, \epsilon_r, \epsilon_z, \gamma} + \frac{1}{\rho}\sigma_\varphi \right] d\epsilon_\varphi + \left[T\left(\frac{\partial A}{\partial \epsilon_z}\right)_{T, \epsilon_r, \epsilon_\varphi, \gamma} + \frac{1}{\rho}\sigma_z \right] d\epsilon_z$$

$$+ \left[T\left(\frac{\partial A}{\partial \gamma}\right)_{T, \epsilon_r, \epsilon_\varphi, \epsilon_z} + \frac{1}{\rho}\tau \right] d\gamma \qquad (7)$$

where $C_{\epsilon_r, \epsilon_\varphi, \epsilon_z, \gamma}$ is the specific heat at constant deformation. To eliminate the entropy from Equation (7) the definition of the Helmholtz function, a, is required and its differential is given by

$$da = \frac{1}{\rho}\left(\sigma_r d\epsilon_r + \sigma_\varphi d\epsilon_\varphi + \sigma_z d\epsilon_z + \tau d\gamma\right) - A\, dT \qquad (8)$$

Noting that the differentials appearing in Equation (8) are exact the following Maxwell relations suitable for solids are obtained:

$$-\left(\frac{\partial A}{\partial \epsilon_r}\right)_{T, \epsilon_\varphi, \epsilon_z, \gamma} = \frac{1}{\rho}\left(\frac{\partial \sigma_r}{\partial T}\right)_{\epsilon_r, \epsilon_\varphi, \epsilon_z, \gamma}$$

$$-\left(\frac{\partial A}{\partial \epsilon_\varphi}\right)_{T, \epsilon_r, \epsilon_z, \gamma} = \frac{1}{\rho}\left(\frac{\partial \sigma_\varphi}{\partial T}\right)_{\epsilon_r, \epsilon_\varphi, \epsilon_z, \gamma}$$

$$-\left(\frac{\partial A}{\partial \epsilon_z}\right)_{T, \epsilon_r, \epsilon_\varphi, \gamma} = \frac{1}{\rho}\left(\frac{\partial \sigma_z}{\partial T}\right)_{\epsilon_r, \epsilon_\varphi, \epsilon_z, \gamma}$$

$$-\left(\frac{\partial A}{\partial \gamma}\right)_{T, \epsilon_r, \epsilon_\varphi, \epsilon_z} = \frac{1}{\rho}\left(\frac{\partial \tau}{\partial T}\right)_{\epsilon_r, \epsilon_\varphi, \epsilon_z, \gamma} \qquad (9)$$

Finally substitution of Equation (9) into Equation (7) yields

$$d\bar{u} = C\, dT + \frac{1}{\rho}\left[-T\left(\frac{\partial \sigma_r}{\partial T}\right) + \sigma_r\right] d\epsilon_r + \frac{1}{\rho}\left[-T\left(\frac{\partial \sigma_\varphi}{\partial T}\right) + \sigma_\varphi\right] d\epsilon_\varphi$$

$$+ \frac{1}{\rho}\left[-T\left(\frac{\partial \sigma_z}{\partial T}\right) + \sigma_z\right] d\epsilon_z + \frac{1}{\rho}\left[-T\left(\frac{\partial \tau}{\partial T}\right) + \tau\right] d\gamma \qquad (10)$$

where subscripts have been omitted but evaluation of partial derivatives at constant deformation is implied.

The strains are related to the displacements in the same manner as in isothermal elasticity since purely geometrical considerations are involved; the pertinent equations are as follows:

$$\epsilon_r = \frac{\partial u}{\partial r}$$

$$\epsilon_\varphi = \frac{u}{r}$$

$$\epsilon_z = \frac{\partial w}{\partial z}$$

$$\gamma = \frac{\partial u}{\partial z} + \frac{\partial w}{\partial r} \tag{11}$$

Substitution of Equations (10) and (11) into Equation (4) yields the following form of the energy equation:

$$\rho c \frac{\partial T}{\partial t} - T\left[\frac{\partial \sigma_r}{\partial T} \frac{\partial \epsilon_r}{\partial t} + \frac{\partial \sigma_\varphi}{\partial T} \frac{\partial \epsilon_\varphi}{\partial t} + \frac{\partial \sigma_z}{\partial T} \frac{\partial \epsilon_z}{\partial t} + \frac{\partial \tau}{\partial T} \frac{\partial \gamma}{\partial t} \right] = -\frac{1}{r} \frac{\partial}{\partial r}(r q_r) - \frac{\partial q_z}{\partial z} \tag{12}$$

To complete the formulation constitutive relations are necessary to furnish a sufficient number of equations among the dependent variables. The relationships given by Fourier's conduction law and Hook's generalized stress-strain law are

$$q_r = -k \frac{\partial T}{\partial r}$$

$$q_z = -k \frac{\partial T}{\partial z} \tag{13}$$

and

$$\epsilon_r = \frac{1}{E}[\sigma_r - \nu(\sigma_\varphi + \sigma_z)] + \beta T$$

$$\epsilon_\varphi = \frac{1}{E}[\sigma_\varphi - \nu(\sigma_z + \sigma_r)] + \beta T$$

$$\epsilon_z = \frac{1}{E}[\sigma_z - \nu(\sigma_r + \sigma_\varphi)] + \beta T$$

$$\gamma = \frac{1}{G} \tau \tag{14}$$

or solving for stress

$$\sigma_r = 2G\left(\epsilon_r + \frac{\nu}{1-2\nu}e - \frac{1+\nu}{1-2\nu}\beta T\right)$$
$$\sigma_\phi = 2G\left(\epsilon_\phi + \frac{\nu}{1-2\nu}e - \frac{1+\nu}{1-2\nu}\beta T\right)$$
$$\sigma_z = 2G\left(\epsilon_z + \frac{\nu}{1-2\nu}e - \frac{1+\nu}{1-2\nu}\beta T\right)$$
$$\tau = G\gamma \qquad (15)$$

where k denotes the thermal conductivity, E the modulus of elasticity, ν Poissons ratio, β the thermal coefficient of expansion, and e the cubical dilatation ($e = \epsilon_r + \epsilon_\phi + \epsilon_z$) .

Making use of the constitutive equations, the coupled governing equations are written in terms of temperature and displacement as follows:

$$\nabla^2 u - \frac{u}{r^2} + \frac{1}{1-2\nu}\frac{\partial e}{\partial r} - 2\left(\frac{1+\nu}{1-2\nu}\right)\beta\frac{\partial T}{\partial r} + \frac{R}{G} = \frac{\rho}{G}\frac{\partial^2 u}{\partial t^2} \qquad (16)$$

$$\nabla^2 w + \frac{1}{1-2\nu}\frac{\partial e}{\partial z} - 2\left(\frac{1+\nu}{1-2\nu}\right)\beta\frac{\partial T}{\partial z} + \frac{Z}{G} = \frac{\rho}{G}\frac{\partial^2 w}{\partial t^2} \qquad (17)$$

$$\rho C\frac{\partial T}{\partial t} + 2G\left(\frac{1+\nu}{1-2\nu}\right)\beta T\frac{\partial e}{\partial t} = \frac{1}{r}\frac{\partial}{\partial r}\left(kr\frac{\partial T}{\partial r}\right) + \frac{\partial}{\partial z}\left(k\frac{\partial T}{\partial z}\right) \qquad (18)$$

where $e = \nabla\cdot\vec{V}$ and ∇^2 denotes the Laplacian in cylindrical coordinates. Various simplifications of the coupled theory are discussed by numerous authors, e.g. Boley and Weiner.[3] In most commonly encountered problems the effect of mechanical coupling and inertia is negligible. Neglecting these effects Equations (16), (17) and (18) become

$$\nabla^2 u - \frac{u}{r^2} + \frac{1}{1-2\nu}\frac{\partial e}{\partial r} - 2\left(\frac{1+\nu}{1-2\nu}\right)\beta\frac{\partial T}{\partial r} + \frac{R}{G} = 0 \qquad (19)$$

$$\nabla^2 w + \frac{1}{1-2\nu}\frac{\partial e}{\partial z} - 2\left(\frac{1+\nu}{1-2\nu}\right)\beta\frac{\partial T}{\partial z} + \frac{Z}{G} = 0 \qquad (20)$$

$$\rho C\frac{\partial T}{\partial t} = \frac{1}{r}\frac{\partial}{\partial r}\left(kr\frac{\partial T}{\partial r}\right) + \frac{\partial}{\partial z}\left(k\frac{\partial T}{\partial z}\right) \qquad (21)$$

respectively, which constitute the uncoupled quasi-static theory. Most problems are solved using this theory. For unsteady problems the time variable then appears only as a parameter in Equations (19) and (20) and therefore simplifies the problem considerably. For steady problems time disappears altogether and the coupled formulation reduces to the quasi-static formulation. The following analysis applies to the quasi-static theory and non-thermal body forces are omitted.

By virtue of the linearity of the problem the solution of Equations (19) and (20) can be written as the sum of two solutions

$$\begin{aligned} u &= u_p + u_c \\ w &= w_p + w_c \end{aligned} \tag{22}$$

where the p subscript denotes a particular solution and c denotes the complimentary solution of the homogeneous equations. A particular solution is given by Goodier[6] in terms of a scalar displacement potential which is defined by

$$\begin{aligned} u_p &= \frac{\partial \psi}{\partial r} \\ w_p &= \frac{\partial \psi}{\partial z} \end{aligned} \tag{23}$$

The Goodier potential then satisfies the relation

$$\nabla^2 \psi = \left(\frac{1+\nu}{1-\nu}\right) \beta T \tag{24}$$

which is obtained by substitution of Equation (23) into Equations (19) and (20). The complimentary solution is given by use of the third component of either the vector displacement potential of Love[10] -- Galerkin[5]

$$u_c = -\frac{\partial^2 \chi}{\partial r \partial z}$$

$$w_c = 2(1-\nu)\nabla^2 \chi - \frac{\partial^2 \chi}{\partial z^2} \tag{25}$$

or that of Boussinesq[4]--Papkovich[12]

$$u_c = -z\frac{\partial \Lambda}{\partial r}$$

$$w_c = 4(1-\nu)\nabla^2 \Lambda - \frac{\partial}{\partial z}(z\Lambda) \tag{26}$$

These potentials satisfy the biharmonic and harmonic equations

$$\nabla^2 \nabla^2 \chi = 0 \tag{27}$$

$$\nabla^2 \Lambda = 0 \tag{28}$$

respectively. Finally the stresses may be written in terms of potentials by combining the particular and complimentary solutions. In terms of Goodier and Love--Galerkin potentials the stresses are

$$\sigma_r = 2G\left[\left(\frac{\partial^2 \psi}{\partial r^2} - \nabla^2 \psi\right) + \frac{\partial}{\partial z}\left(\nu \nabla^2 \chi - \frac{\partial^2 \chi}{\partial r^2}\right)\right]$$

$$\sigma_\phi = 2G\left[\left(\frac{1}{r}\frac{\partial \psi}{\partial r} - \nabla^2 \psi\right) + \frac{\partial}{\partial z}\left(\nu \nabla^2 \chi - \frac{1}{r}\frac{\partial \chi}{\partial r}\right)\right]$$

$$\sigma_z = 2G\left[\left(\frac{\partial^2 \psi}{\partial z^2} - \nabla^2 \psi\right) + \frac{\partial}{\partial z}\left([2-\nu]\nabla^2 \chi - \frac{\partial^2 \chi}{\partial z^2}\right)\right]$$

$$\tau = 2G\left[\frac{\partial^2 \psi}{\partial r \partial z} + \frac{\partial}{\partial r}\left([1-\nu]\nabla^2 \chi - \frac{\partial^2 \chi}{\partial z^2}\right)\right] \tag{29}$$

and in terms of Goodier and Boussinesq--Papkovich potentials they are

$$\sigma_r = 2G\left[\left(\frac{\partial^2\psi}{\partial r^2} - \nabla^2\psi\right) + 2\nu\frac{\partial\Lambda}{\partial z} - z\frac{\partial^2\Lambda}{\partial r^2}\right]$$

$$\sigma_\phi = 2G\left[\left(\frac{1}{r}\frac{\partial\psi}{\partial r} - \nabla^2\psi\right) + 2\nu\frac{\partial\Lambda}{\partial z} - \frac{z}{r}\frac{\partial\Lambda}{\partial r}\right]$$

$$\sigma_z = 2G\left[\left(\frac{\partial^2\psi}{\partial z^2} - \nabla^2\psi\right) + 2(1-\nu)\frac{\partial\Lambda}{\partial z} - z\frac{\partial^2\Lambda}{\partial z^2}\right]$$

$$\tau = 2G\left[\frac{\partial^2\psi}{\partial r\partial z} + (1-2\nu)\frac{\partial\Lambda}{\partial r} - z\frac{\partial^2\Lambda}{\partial r\partial z}\right] \qquad (30)$$

2. The Temperature Problem

The following assumptions are made:

1) Axial conduction in the tube wall and fluid is neglected. The effect of axial conduction in the wall is discussed in Appendix C. Schneider[16] investigated the effect in the fluid and showed that the effect is negligible when the Peclet number (Reynolds number times Prandtl number) is greater than 100. Because of the low Prandtl numbers of liquid metals (.003-.03) axial conduction may become important for this class of fluids.

2) The physical properties are constant.

3) The fluid has a fully developed laminar velocity profile.

4) The external convection heat transfer coefficient is constant.

5) The fluid temperature is uniform at the entrance.

6) The ambient is isothermal.

7) The fluid is incompressible.

A schematic of the physical model is shown in Figure 20. Under the assumptions given above the governing differential equations are derived in Appendix A. The resulting dimensionless formulation is given by

$$\frac{\partial}{\partial R}\left(R\,\frac{\partial \phi}{\partial R}\right) = 0 \tag{31}$$

$$Pe\,(1-R^2)\,\frac{\partial \theta}{\partial Z} = \frac{1}{R}\,\frac{\partial}{\partial R}\left(R\,\frac{\partial \theta}{\partial r}\right) \tag{32}$$

subject to the boundary conditions

$$\phi(1, Z) = \theta(1, Z) \tag{33a}$$

$$\frac{\partial \phi}{\partial R}(R_0, Z) = -\frac{B}{R_0}\,\phi(R_0, Z) \tag{33b}$$

$$\theta(R, 0) = 1 \tag{33c}$$

$$\frac{\partial \theta}{\partial R}(0, Z) = 0 \tag{33d}$$

$$\frac{\partial \theta}{\partial R}(1, Z) = -N\,\theta(1, Z) \tag{33e}$$

where R and Z denote the dimensionless radial and axial coordinate, respectively, ϕ and θ the dimensionless temperature of the wall and fluid, respectively, Pe the Peclet number, B modified Biot number, and N modified Nusselt number.

B. Solution

1. Temperature Solution

The temperature distribution in the tube is determined from Equation (31) subject to the boundary conditions Equations (33a) and (33b). The simple solution is readily obtained as

$$\phi(R, Z) = \left[1 - \bar{B} \ln R\right]\theta(1, Z) \tag{34}$$

where $\bar{B} = \dfrac{B}{1 + B \ln R_0}$.

Determination of the inside surface temperature requires solution of the convection problem.

The solution of the convection problem is found from Equation (32) subject to Equations (33c), (33d), and (33e). Applying the separation of variables a product solution is assumed in the form

$$\theta = \xi(z)\, \mathcal{R}(R) \tag{35}$$

and substituted into Equation (32). This yields the two ordinary differential equations

$$\frac{d\xi}{dz} + \frac{\lambda^2}{Pe}\,\xi = 0 \tag{36}$$

$$\frac{d}{dR}\left(R\,\frac{d\mathcal{R}}{dR}\right) + \lambda^2 R(1-R^2)\,\mathcal{R} = 0 \tag{37}$$

where λ is an arbitrary real constant of separation. Substitution of Equation (35) into the boundary conditions, Equations (33c), (33d), and (33e), yields

$$\xi(0)\,\mathcal{R}(R) = 1 \tag{38a}$$

$$\frac{d\mathcal{R}(0)}{dR} = 0 \tag{38b}$$

$$\frac{d\mathcal{R}(1)}{dR} = -N\,\mathcal{R}(1) \tag{38c}$$

The solution of Equation (36) is well known and can be written immediately as

$$\xi(z) = C_1\, e^{-\frac{\lambda^2}{Pe} z} \tag{39}$$

where C_1 is an arbitrary constant. The solution of Equation (37), however, cannot be expressed in terms of previously tabulated functions.

Therefore solution requires computation of the eigenfunctions and eigenvalues of the system which is of the Sturm-Liouville type.

A power series solution of Equation (37) can be written in the form

$$\mathcal{R} = \sum_{n=0}^{\infty} a_n R^n \tag{40}$$

where $a_{2m-1} = 0$ and $a_{2m} = -\frac{\lambda^2}{2m^2}(a_{2m-2} - a_{2m-4})$. The characteristic values, λ_m, are then the roots of the polynomial obtained by substitution of Equation (40) into Equation (38c). However, in practice, only the first few roots of this polynomial can conveniently be determined.

Instead of using the power series method of solution a more direct numerical procedure was used in the actual numerical computations. The differential equation, Equation (37), was integrated numerically using the Runga-Kutta method. Eigenvalues were determined with a successive approximation procedure. After integration over the domain for a trial value of λ_m appropriate values of $\mathcal{R}(1)$ and $\frac{d\mathcal{R}(1)}{dR}$ were substituted into the boundary condition, Equation (38c). For the correct value of λ_m Equation (38c) becomes an identity. The eigenfunction was determined by a final Runga-Kutta integration using the appropriate eigenvalue.

Having determined the eigenfunctions and eigenvalues the general solution of the convection problem may be written as

$$\theta(R,z) = \sum_{n=0}^{\infty} A_n \mathcal{R}_n(R)\, e^{-\frac{\lambda_n^2}{Pe} z} \tag{41}$$

The A_m are constants to be determined in such a way that the remaining

non-separable boundary condition is satisfied. Substituting Equation (41) into Equation (38a), multiplying through by $R(1-R^2)\mathcal{R}_m$, and integrating the resulting expression from 0 to 1 yields

$$A_m = \frac{\int_0^1 R(1-R^2)\mathcal{R}_m \, dR}{\int_0^1 R(1-R^2)\mathcal{R}_m^2 \, dR} \tag{42}$$

It is noted that the $\mathcal{R}_m$ are orthogonal with respect to the weighting function $R(1-R^2)$ on the interval 0 to 1. Successive application of Simpson's rule is then used to evaluate numerically the integrals appearing in Equation (42). Finally the temperature of the fluid at the inside wall is given by

$$\theta(1,z) = \sum_{n=0}^{\infty} B_n e^{-\mu_n z} \tag{43}$$

where $B_m = A_m \mathcal{R}_m(1)$ and $\mu_m = \frac{\lambda_m^2}{Pe}$

Values of the eigenvalues, λ_m, eigenfunctions at the wall, $\mathcal{R}_m(1)$, and coefficients, A_m and B_m, are tabulated in Appendix D for N = 20, 17, 6, 2, 1, and 0.5. It was found feasible to carry the computations as far as the first 20 terms of the series. All computations were performed on an IBM 7090 computer.

Comparison of the numerical results was made with those of Schenk and Dumore[15] for the first three terms of the series. Good agreement was found for the eigenvalues and eigenfunctions while some of the coefficients showed minor discrepencies. It is noted that the nomenclature in their paper is related to the notation used here by $\beta_m = 2\lambda_m$ and $Nu' = 2N$.

Solutions obtained by separation of variables and Fourier series are "large time" solutions and thus slowly convergent for "small time". Therefore an asymptotic solution valid at the entrance is obtained.

Based on the physical model shown in Figure 21 the governing differential equations are derived in Appendix B. The resulting dimensionless formulation is given by

$$y \frac{\partial \theta}{\partial \bar{z}} = \frac{\partial^2 \theta}{\partial y^2} \tag{44}$$

subject to

$$\theta(y, 0) = 0 \tag{45a}$$

$$\theta(\infty, \bar{z}) = 0 \tag{45b}$$

$$\frac{\partial \theta}{\partial y}(0, \bar{z}) = N[\theta(0, \bar{z}) - 1] \tag{45c}$$

where θ denotes the dimensionless fluid temperature, y and $\bar{z}$ the dimensionless transverse and axial coordinates, respectively, and N a modified Nusselt number.

A solution may readily be obtained by the use of Laplace transforms. Taking the Laplace transform of Equations (44) and (45) with respect to the dimensionless axial coordinate $\bar{z}$ yields

$$\frac{d^2 \bar{\theta}}{dy^2}(y, s) - s y \bar{\theta}(y, s) = 0 \tag{46}$$

subject to the boundary conditions

$$\bar{\theta}(\infty, s) = 0 \tag{47a}$$

$$\frac{d\bar{\theta}}{dy}(0,s) = N\left[\bar{\theta}(0,s) - \frac{1}{s}\right] \tag{47b}$$

where s is the transform parameter and $\bar{\theta}(y,s)$ the transformed temperature.

The solution of Equation (46), noting that $\lim_{x\to\infty} I_\nu(x) \to \infty$, may be written as

$$\bar{\theta}(y,s) = A\, y^{1/2}\, K_{1/3}\left(\tfrac{2}{3}\, s^{1/2}\, y^{3/2}\right) \tag{48}$$

which satisfies Equation (47a). The functions $I_\nu(x)$ and $K_\nu(x)$ are the modified Bessel functions of the first and second kind, respectively, of order ν and argument x. The constant A is found by substitution of Equation (48) into Equation (47b) and is given by

$$A = \frac{C_1}{s^{7/6}\left(1 + C_2 s^{-1/3}\right)} \tag{49}$$

where $C_1 = \dfrac{2N}{3^{2/3}\,\Gamma(2/3)}$, $C_2 = \dfrac{N\,\Gamma(1/3)}{3^{1/3}\,\Gamma(2/3)}$,

and $\Gamma(x)$ denotes the Gamma function of argument x.

Having obtained a solution of the transformed formulation the transformed wall temperature is obtained by taking the limit of Equation (48) as y approaches zero. The result is

$$\bar{\theta}(0,s) = \frac{C}{s^{4/3}\left(1 + C s^{-1/3}\right)} \tag{50}$$

where $C = \dfrac{N\,\Gamma(1/2)}{3^{1/3}\,\Gamma(2/3)}$

Since a solution which is rapidly convergent in the entrance region is desired, a "small $\bar{z}$" solution is obtained by noting that large values of the transform parameter s correspond to small values of $\bar{z}$. Consequently, the expansion of the transformed solution into

a series of ascending powers of $\frac{1}{f(s)}$ and subsequent term-by-term inversion gives a solution useful for small values of $\bar{z}$ (see for instance, Arpaci[1]). In the above, $f(s)$ is a function of s whose form is determined by the particular form of the solution under study.

Before proceeding recall that the sum of a geometric series is given by

$$\frac{1}{1-f(s)} = 1 + f(s) + f^2(s) + \cdots ; \quad |f(s)| < 1 \qquad (51)$$

Choosing $f(s) = -c\, s^{-1/3}$ and substituting into Equation (51) yields

$$\frac{1}{(1+c\, s^{-1/3})} = 1 - (c\, s^{-1/3}) + (c\, s^{-1/3})^2 - \cdots \qquad (52)$$

Substitution of Equation (52) into Equation (50) and rearrangement of terms then produces

$$\bar{\theta}(0,s) = c\left(s^{-4/3} - c\, s^{-5/3} + c^2 s^{-2} - c^3 s^{-7/3} + \cdots \right) \qquad (53)$$

Referring to published tables of Laplace transform pairs the transformed solution can now be inverted term-by-term. The wall temperature is therefore given by

$$\theta(0,\bar{z}) = \sum_{m=1}^{\infty} \frac{(-1)^{m-1} \left(c\, \bar{z}^{1/3}\right)^m}{\Gamma\left(1+\frac{m}{3}\right)} \qquad (54)$$

Referring the wall temperature to T_∞ instead of T_0, Equation (54) may be rearranged to give

$$\theta^*(0,\bar{z}) = 1 + \sum_{m=1}^{\infty} \frac{(-1)^m \left(c\, \bar{z}^{1/3}\right)^m}{\Gamma\left(1+\frac{m}{3}\right)} \qquad (55)$$

were $\theta^* = \frac{T_f - T_\infty}{T_0 - T_\infty}$

2. Stress Solution

A particular solution is found using Goodiers thermoelastic displacement potential by examination of the particular form of the temperature expression. Once the particular solution is found a Biharmonic Love-Galerkin function is obtained.

For convenience the exact temperature distribution in the wall is written here as

$$\phi(R,z) = (1 - \bar{B} \ln R) \sum_{n=0}^{\infty} B_n e^{-\mu_n z} \tag{56}$$

By inspection of Equation (56) one can construct a particular solution to Equation (24). It can thus be verified by direct substitution that

$$\psi_n = M_n (1 - \bar{B} \ln R) e^{-\mu_n z} \tag{57}$$

is a particular solution of Equation (24), where ψ_n is the Goodier potential corresponding to the n-th term of Equation (56) and $M_n = \left(\frac{1+\nu}{1-\nu}\right) \frac{\beta(T_0 - T_\infty)}{\mu_n^2} B_n$. By adding all of the particular solutions of the form Equation (57) one obtains

$$\psi = (1 - \bar{B} \ln R) \sum_{n=0}^{\infty} M_n e^{-\mu_n z} \tag{58}$$

One can obtain a solution of the biharmonic equation by writing Equation (27) as a system of two second order partial differential equations given by

$$\nabla^2 \chi = f \tag{59a}$$

$$\nabla^2 f = 0 \tag{59b}$$

where f is an intermediate function. (see for instance, Arpaci[2])

Using separation of variables and noting that $\lim_{z\to\infty} e^{+\mu_n z} = \infty$ the solution of Equation (59b) being well known is written immediately as

$$f_n(R,z) = \begin{pmatrix} J_0(\mu_n R) \\ Y_0(\mu_n R) \end{pmatrix} e^{-\mu_n z} \tag{60}$$

where J_0 and Y_0 are the ordinary Bessel functions of the first and second kind, respectively, of zero order and μ_n is the separation parameter which was defined in the temperature solution. Substitution of Equation (60) into Equation (59a) yields

$$\nabla^2 \chi_n = \begin{pmatrix} J_0(\mu_n R) \\ Y_0(\mu_n R) \end{pmatrix} e^{-\mu_n z} \tag{61}$$

Since the right hand side of Equation (61) is composed of product terms a convenient form of the Love--Galerkin function can be written as

$$\chi_n = \begin{pmatrix} J_0(\mu_n R) & , & R\,J_1(\mu_n R) \\ Y_0(\mu_n R) & , & R\,Y_1(\mu_n R) \end{pmatrix} e^{-\mu_n z} \tag{62}$$

This relation was chosen because $\begin{pmatrix} R\,J_1(\mu_n R) \\ R\,Y_1(\mu_n R) \end{pmatrix} e^{-\mu_n z}$ are known to be biharmonic functions.

Another approach to determining χ is to assume a separable solution of the form $\chi(R,z) = F(R)\, e^{-\mu_n z}$ and substitute into Equation (61). The complimentary solutions of this equation are $J_0(\mu_n R)$ and $Y_0(\mu_n R)$ and a particular solution may be obtained by variation of parameters. However, it is expedient to return to Equation (2) and proceed from there.

A solution of the biharmonic equation in terms of four arbitrary constants a_n, b_n, c_n, and d_n is written in the form

$$\chi_n = \left[a_n J_0(\mu_n R) + b_n Y_0(\mu_n R) + c_n R J_1(\mu_n R) + d_n R Y_1(\mu_n R)\right] e^{-\mu_n z} \tag{63}$$

where the n subscript refers to the nth term corresponding to the particular solution. Summing over all terms one obtains

$$\chi = \sum_{n=0}^{\infty} \left[a_n J_0(\mu_n R) + b_n Y_0(\mu_n R) + c_n R J_1(\mu_n R) + d_n R Y_1(\mu_n R) \right] e^{-\mu_n z} \tag{64}$$

The stresses are obtained by substitution of Equations (58) and (64) into Equation (29). After expanding and combining terms the stresses in dimensionless form are given by

$$\begin{aligned} \sigma_r^* = \sum_{n=0}^{\infty} \Big\{ & \left(\left[\frac{1}{(\mu_n R)^2} + \ln R \right] \bar{B} - 1 \right) B_n - a_n \left[J_0(\mu_n R) \right. \\ & \left. - \frac{1}{\mu_n R} J_1(\mu_n R) \right] - b_n \left[Y_0(\mu_n R) - \frac{1}{\mu_n R} Y_1(\mu_n R) \right] \\ & + c_n \left[(1-2\nu) J_0(\mu_n R) - \mu_n R J_1(\mu_n R) \right] \\ & + d_n \left[(1-2\nu) Y_0(\mu_n R) - \mu_n R Y_1(\mu_n R) \right] \Big\} e^{-\mu_n z} \end{aligned} \tag{65a}$$

$$\begin{aligned} \sigma_\varphi^* = \sum_{n=0}^{\infty} \Big\{ & -\left(\left[\frac{1}{(\mu_n R)^2} - \ln R \right] \bar{B} + 1 \right) B_n \\ & - a_n \left[\frac{1}{\mu_n R} J_1(\mu_n R) \right] - b_n \left[\frac{1}{\mu_n R} Y_1(\mu_n R) \right] \\ & + c_n \left[(1-2\nu) J_0(\mu_n R) \right] + d_n \left[(1-2\nu) Y_0(\mu_n R) \right] \Big\} e^{-\mu_n z} \end{aligned} \tag{65b}$$

$$\begin{aligned} \sigma_z^* = \sum_{n=0}^{\infty} \Big\{ & a_n \left[J_0(\mu_n R) \right] + b_n \left[Y_0(\mu_n R) \right] \\ & + c_n \left[\mu_n R J_1(\mu_n R) - 2(2-\nu) J_0(\mu_n R) \right] \\ & + d_n \left[\mu_n R Y_1(\mu_n R) - 2(2-\nu) Y_0(\mu_n R) \right] \Big\} e^{-\mu_n z} \end{aligned} \tag{65c}$$

$$\begin{aligned} \tau^* = \sum_{n=0}^{\infty} \Big\{ & \left[\frac{\bar{B}}{\mu_n R} \right] B_n + a_n \left[J_1(\mu_n R) \right] + b_n \left[Y_1(\mu_n R) \right] \\ & - c_n \left[\mu_n R J_0(\mu_n R) + 2(1-\nu) J_1(\mu_n R) \right] \\ & - d_n \left[\mu_n R Y_0(\mu_n R) + 2(1-\nu) Y_1(\mu_n R) \right] \Big\} e^{-\mu_n z} \end{aligned} \tag{65d}$$

where the general dimensionless stress is related to the actual stress by $\sigma^* = \frac{\sigma}{2G\beta (T_o - T_\infty)\left(\frac{1+\nu}{1-\nu}\right)}$, σ being the actual stress.

Since the surfaces are free of externally applied forces or restraints, the boundary conditions are

$$\begin{aligned} \sigma_r(1,z) &= 0 \\ \sigma_r(R_o,z) &= 0 \\ \tau(1,z) &= 0 \\ \tau(R_o,z) &= 0 \end{aligned} \tag{66}$$

The stresses at $z = 0$ are self-equilibriating and Saint Venant's principle applies; for $z \to \infty$ all stresses vanish. Finally substitution of Equations (65a) and (65d) into Equation (66) yields the following four equations in the four unknown coefficients:

$$\begin{aligned} &-\left[J_0(\mu_n) - \tfrac{1}{\mu_n} J_1(\mu_n)\right] a_n - \left[Y_0(\mu_n)\right. \\ &\left. - \tfrac{1}{\mu_n} Y_1(\mu_n)\right] b_n + \left[(1-2\nu) J_0(\mu_n) - \mu_n J_1(\mu_n)\right] c_n \\ &+ \left[(1-2\nu) Y_0(\mu_n) - \mu_n Y_1(\mu_n)\right] d_n = -\left[\frac{\bar{\beta}}{\mu_n^2} - 1\right] B_n \end{aligned} \tag{67a}$$

$$\begin{aligned} &-\left[J_0(\mu_n R_o) - \tfrac{1}{\mu_n R_o} J_1(\mu_n R_o)\right] a_n - \left[Y_0(\mu_n R_o) - \tfrac{1}{\mu_n R_o} Y_1(\mu_n R_o)\right] b_n \\ &+ \left[(1-2\nu) J_0(\mu_n R_o) - \mu_n R_o J_1(\mu_n R_o)\right] c_n + \left[(1-2\nu) Y_0(\mu_n R_o)\right. \\ &\left. - \mu_n R_o Y_1(\mu_n R_o)\right] d_n = -\left\{\left[\left(\tfrac{1}{\mu_n R_o}\right)^2 + \ln R_o\right] \bar{\beta} - 1\right\} B_n \end{aligned} \tag{67b}$$

$$\begin{aligned} &\left[J_1(\mu_n)\right] a_n + \left[Y_1(\mu_n)\right] b_n \\ &-\left[\mu_n J_0(\mu_n) + 2(1-\nu) J_1(\mu_n)\right] c_n \\ &-\left[\mu_n Y_0(\mu_n) + 2(1-\nu) Y_1(\mu_n)\right] d_n = -\frac{\bar{\beta}}{\mu_n} B_n \end{aligned} \tag{67c}$$

$$[J_1(\mu_n R_o)]a_n + [Y_1(\mu_n R_o)]b_n$$

$$-[\mu_n R_o J_o(\mu_n R_o) + 2(1-\nu)J_1(\mu_n R_o)]c_n$$

$$-[\mu_n R_o Y_o(\mu_n R_o) + 2(1-\nu)Y_1(\mu_n R_o)]d_n = -\frac{\bar{B}}{\mu_n R_o} B_n \qquad (67d)$$

The unknown coefficients may be determined by application of Cramers rule and the theory of determinants. However, standard matrix methods of evaluation were used in the actual numerical computations.

C. Results

Representative numerical results are given in the form of graphs and the effect of the various parameters is illustrated. The parameters appearing in the solution are Pe, the Peclet number (Reynolds number times Prandtl number), N, a modified Nusselt number, B, a modified Biot number, and R_o, the ratio of outside to inside tube radius.

The natural parameter in the temperature solution is the dimensionless distance $\frac{z}{Pe}$ which is the inverse of the Graetz number. The Peclet number appearing in this parameter may vary from a high of approximately 10^7 for viscous oils to a low of zero. However, because of the assumptions used in the formulation the solution is useful for Peclet numbers down to approximately 10.

The temperature distribution at the inside wall of the tube is shown in Figure 2 and the effect of modified Nusselt number is illustrated. Values of N may vary from 0 to ∞. The limiting case of $N = 0$ corresponds to an insulated wall and $N = \infty$ corresponds to a constant wall temperature. In this figure as in succeeding ones the

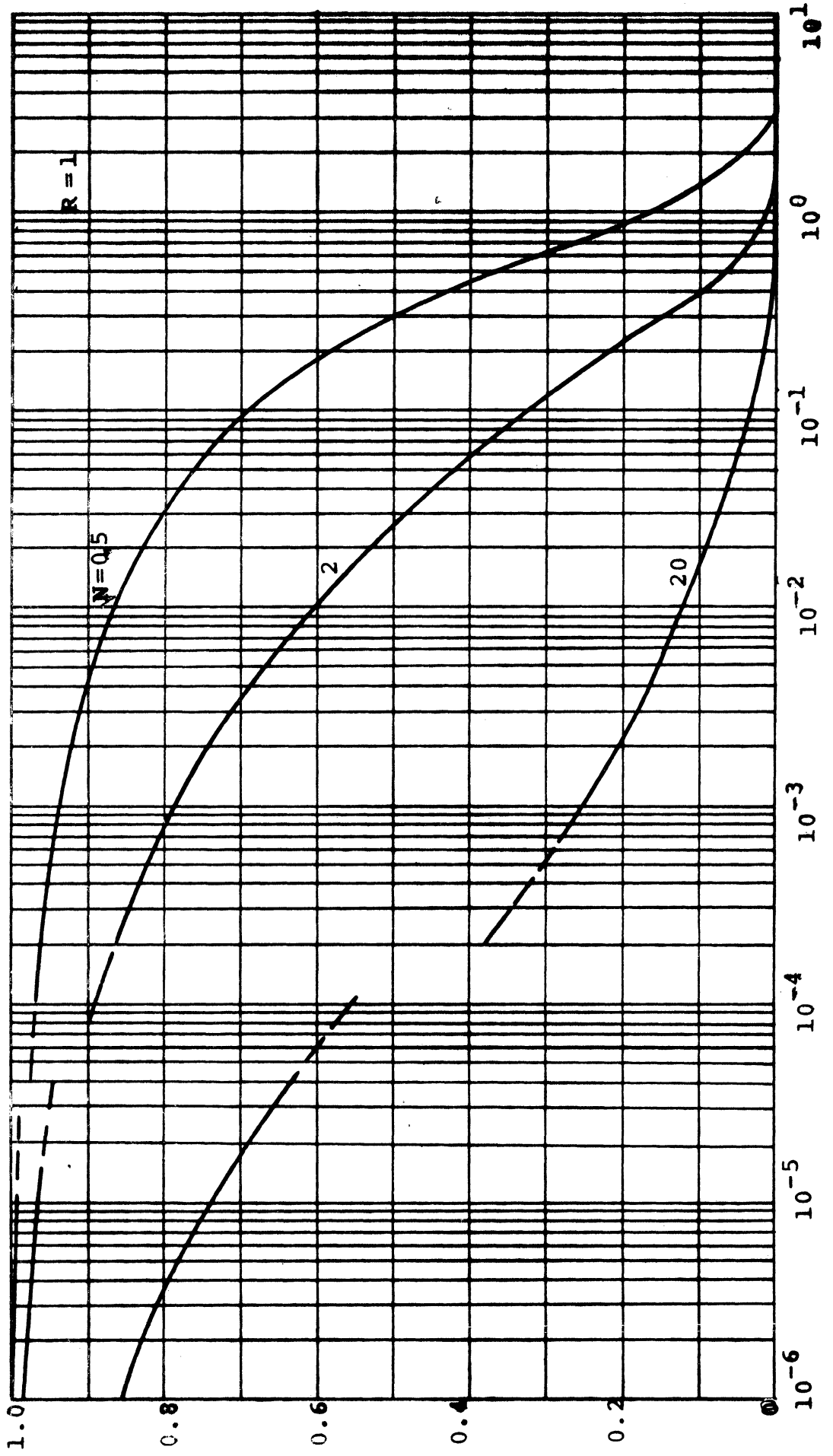

Figure 2. Effect of Modified Nusselt Number on Wall Temperature I. (R = 1)

set of curves for small $\frac{z}{Pe}$ was obtained from the approximate solution and the set for large $\frac{z}{Pe}$ was obtained from the exact solution. In Figure 3 the inside wall temperature is plotted as a function of the dimensionless axial distance, z , for the same values of N .

The Biot number is a measure of the relative importance of the internal thermal resistance of the wall and the external film resistance. As the Biot number increases the relative importance of the thermal resistance of the wall also increases. Values of the Biot number may range from 0 to ∞. Figure 4 illustrates the effect of B on outside wall temperature.

Finally the effect of the wall thickness ratio on outside wall temperature is shown in Figure 5. The temperature drop across the wall increases as R_o increases.

The maximum curvature of the axial temperature profile occurs near the entrance of the tube. Thus the main effect of the axial curvature on the stresses is also confined to this region. In the stress results which follow the plane strain solution is plotted along with the exact solution for reasons of comparison.

In Figures 6 and 7 the axial and tangential stresses at the surface are compared. The stresses behave in a similar manner and the axial stress at the outside surface deviates most from the plain strain case. Therefore, only the effect of the various parameters on the axial stress at $R = R_O$ is shown in the following results. The radial and shear stresses along the coordinate directions are generally much smaller than the maximum axial and tangential stresses and are not given.

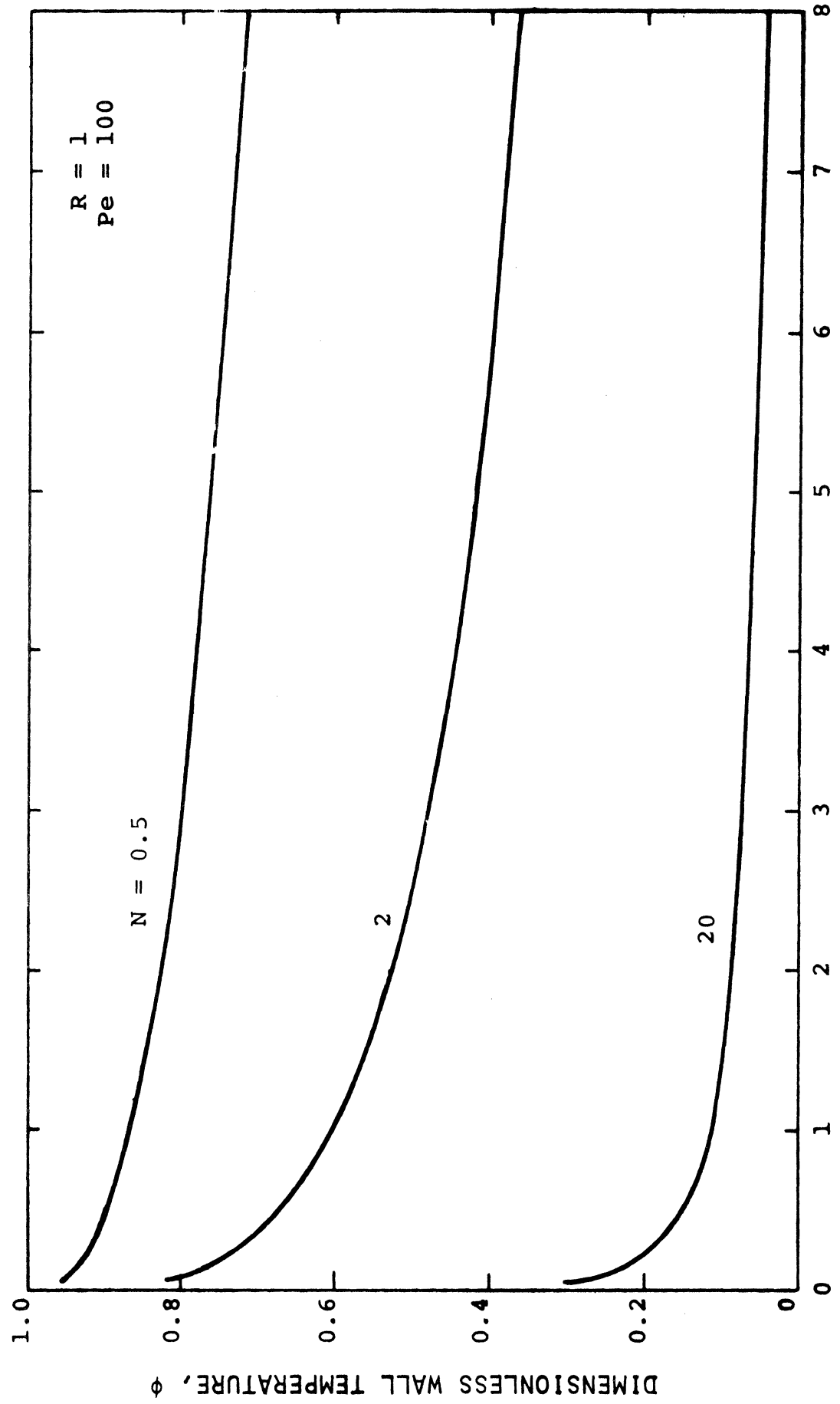

Figure 3. Effect of Modified Nusselt Number on Wall Temperature II. (R = 1, Pe = 100)

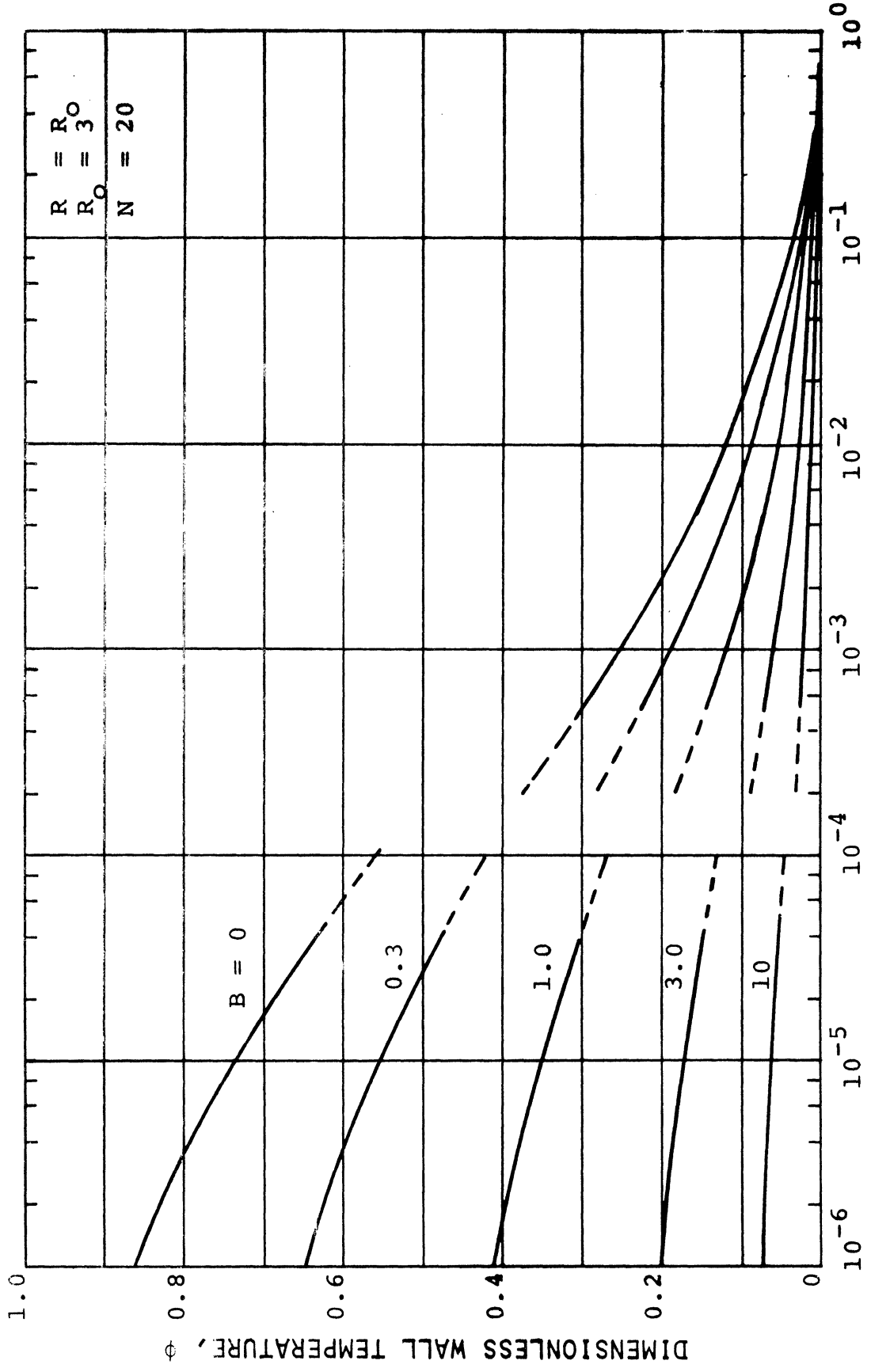

Figure 4. Effect of Modified Biot Number on Wall Temperature. ($R = R_o$, $R_o = 3$, $N = 20$)

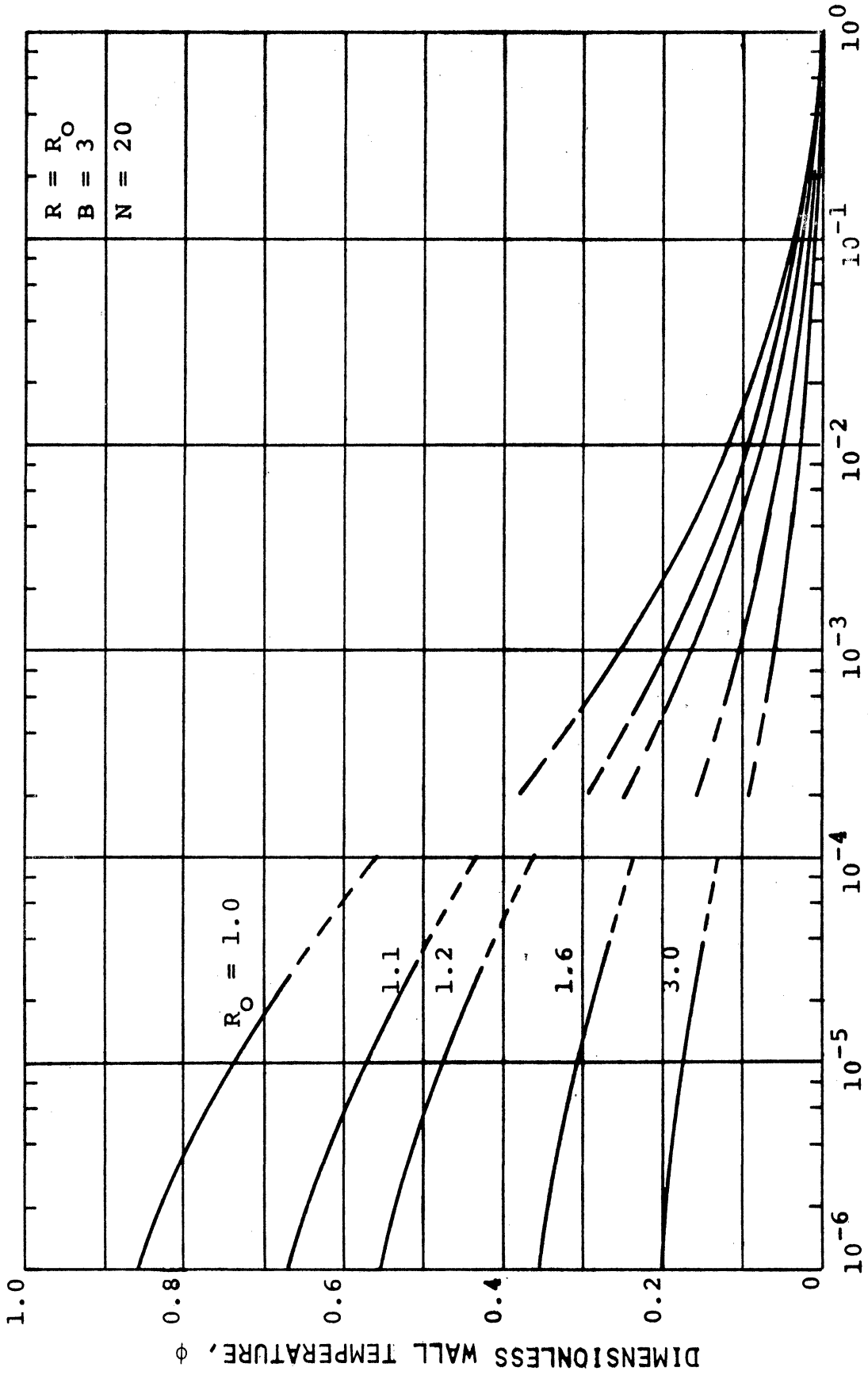

Figure 5. Effect of Tube Geometry on Wall Temperature. ($R = R_o$, B = 3, N = 20)

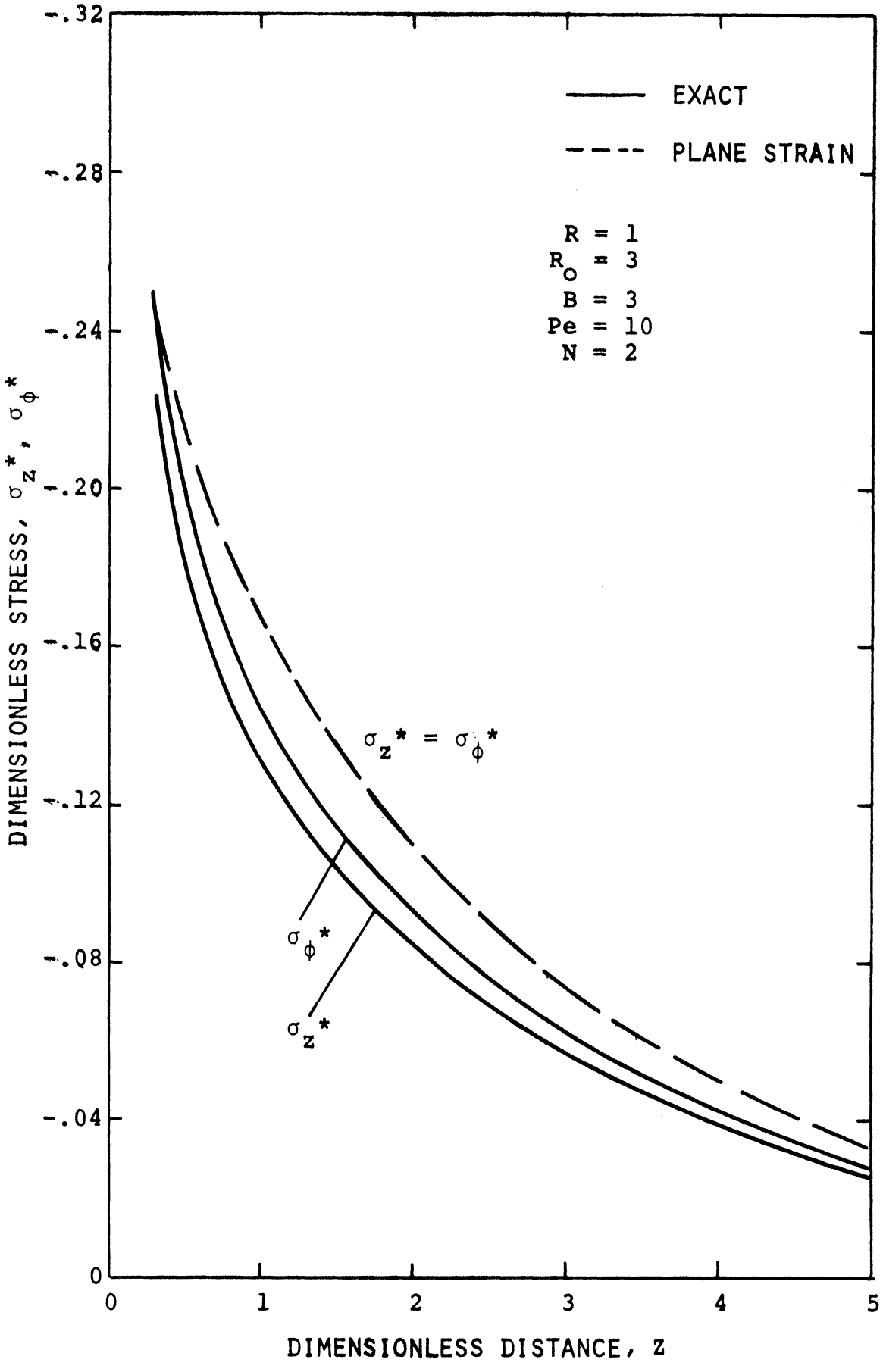

Figure 6. Comparison of Tangential and Axial Stress I. ($R = 1$, $R_o = 3$, $B = 3$, $Pe = 10$, $N = 2$).

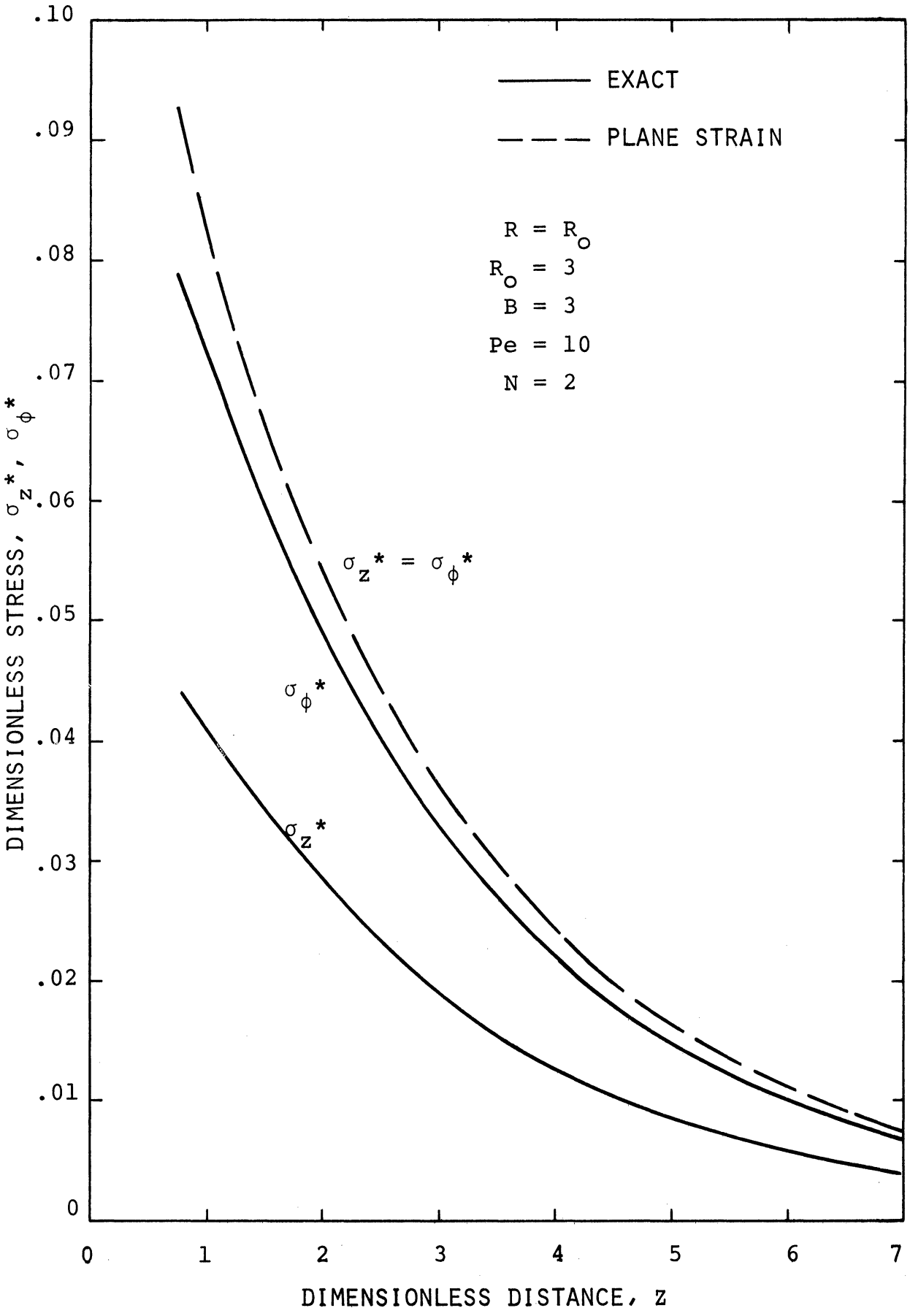

Figure 7. Comparison of Tangential and Axial Stress II. ($R = R_o$, $R_o = 3$, $B = 3$, $Pe = 10$, $N = 2$)

The effect of tube geometry is shown in Figures 8 and 9. As the ratio of outside to inside radius increases the axial effect increases at constant dimensionless distance. Figure 10 shows the stress behavior for various values of the modified Nusselt number. In the limiting cases of $N = 0$ and $N = \infty$ the thermal stresses are zero (neglecting end effects) since the tube wall temperature is uniform. Therefore maximum stresses are obtained for intermediate values of N. Figure 11 shows the effect of Biot number on the stresses. For $B = 0$ the radial gradient is zero and the stresses are the result of the axial gradient. The axial effect decreases as B increases. Finally the influence of the Peclet number is illustrated in Figure 12.

In the plane strain solution the axial variation is carried as a parameter. Thus the plane strain stresses vary as the temperature varies. Figures 13, 14, and 15 illustrate the behavior of the plane strain solution and show the effect of modified Nusselt number, geometry, and modified Biot number, respectively. The plane strain solution is given in Appendix E.

In the numerical computations the number of terms required for convergence of the series solutions varied. Computation was terminated when the last term of the series added was less than .05 percent of the sum. For the exact solution the number of terms required increased as $\frac{z}{Pe}$ decreased and all 20 terms available were used for $\frac{z}{Pe}$ of the order of 5000. The exact number of terms used varied with N , the larger values of N requiring more terms for a given $\frac{z}{Pe}$. For the approximate solution more terms were required as $\frac{z}{Pe}$ increased and up to 50 terms of the series were used.

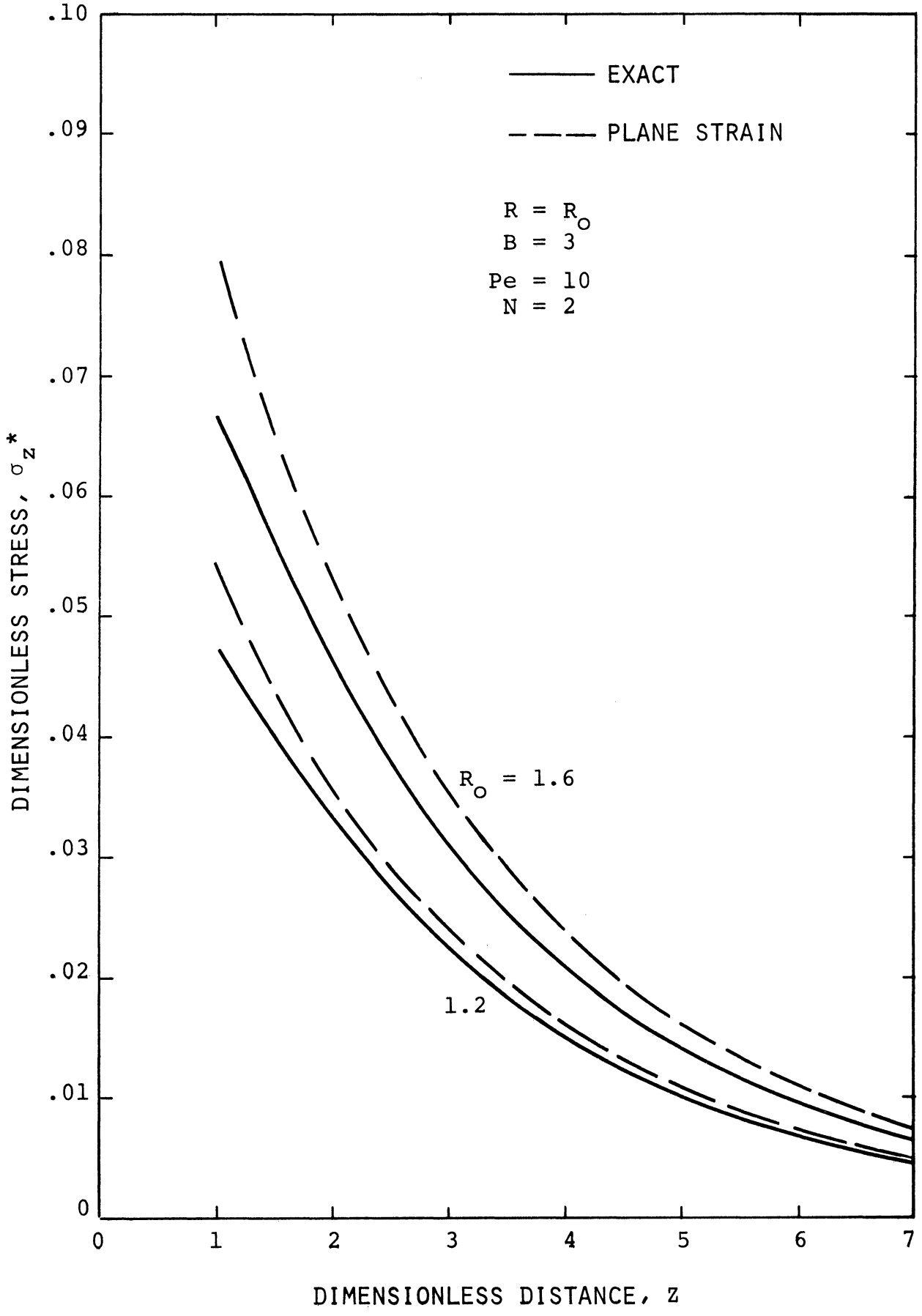

Figure 8. Effect of Tube Geometry on Axial Stress I. ($R = R_o$, $B = 3$, $Pe = 10$, $N = 2$)

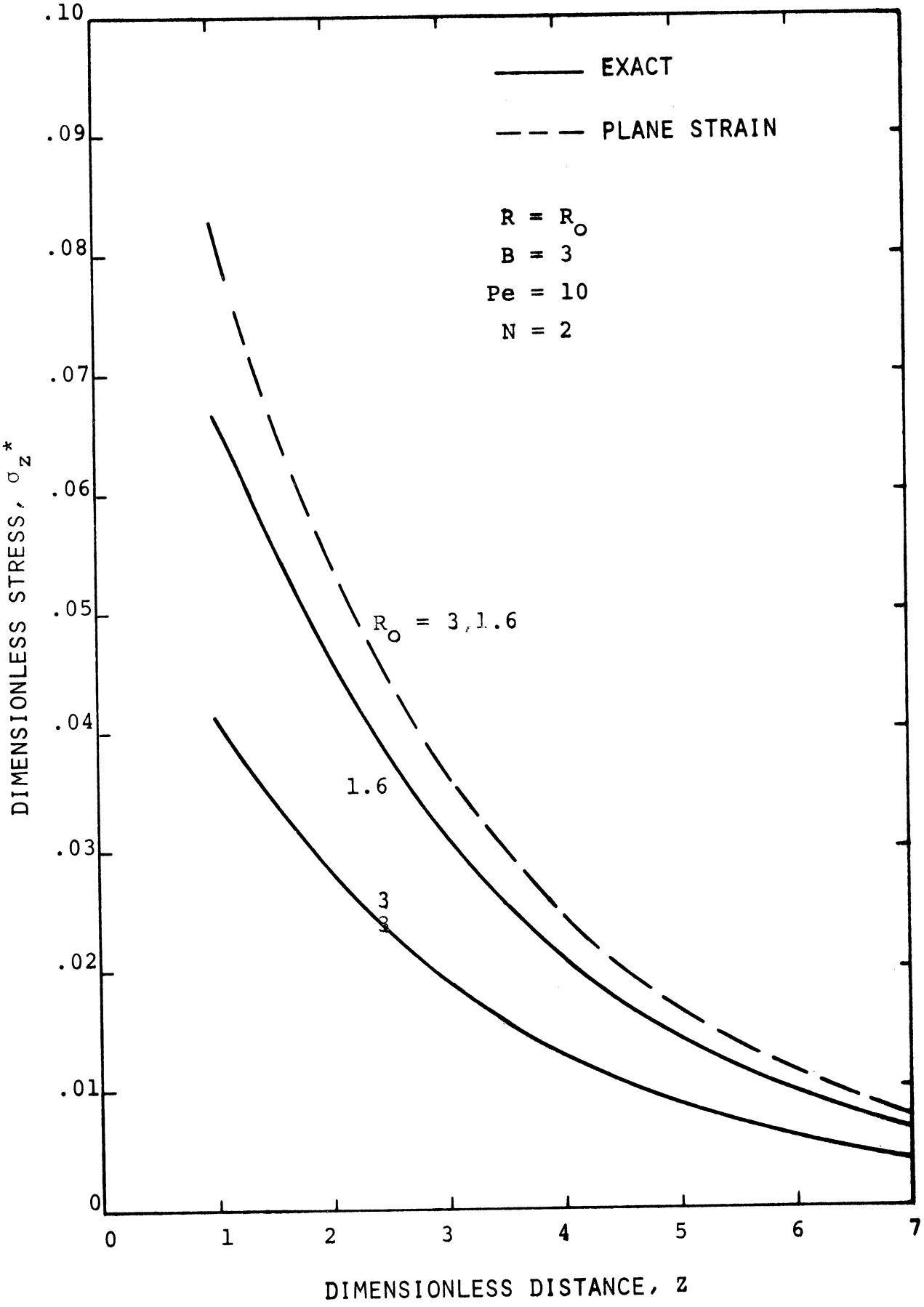

Figure 9. Effect of Tube Geometry on Aixal Stress II. ($R = R_o$, $B = 3$, $Pe = 10$, $N = 2$)

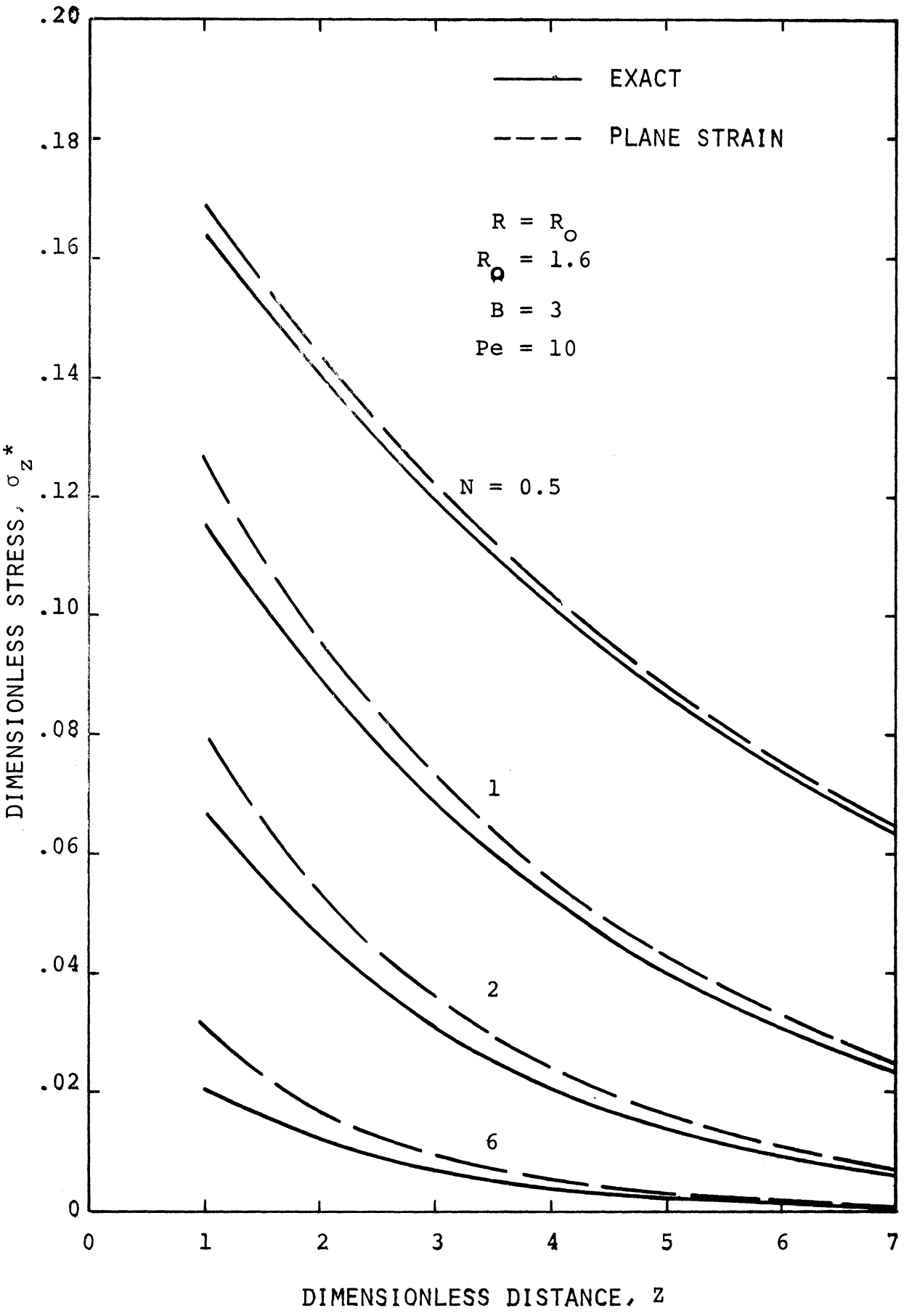

Figure 10. Effect of Modified Nusselt Number on Axial Stress. ($R = R_o$, $R_o = 1.6$, $B = 3$, $Pe = 10$)

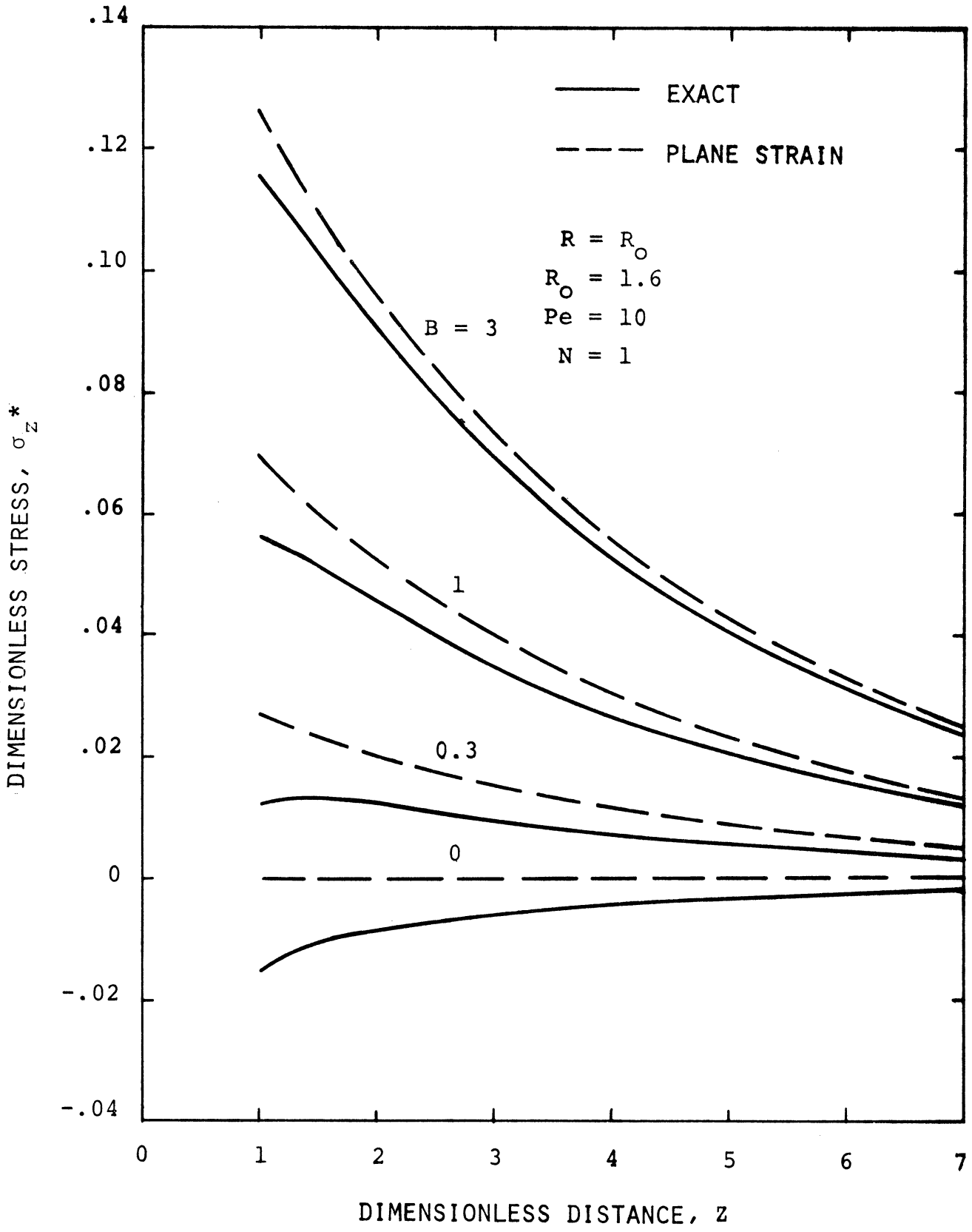

Figure 11. Effect of Modified Biot Number on Axial Stress. ($R = R_o$, $R_o = 1.6$, $Pe = 10$, $N = 1$)

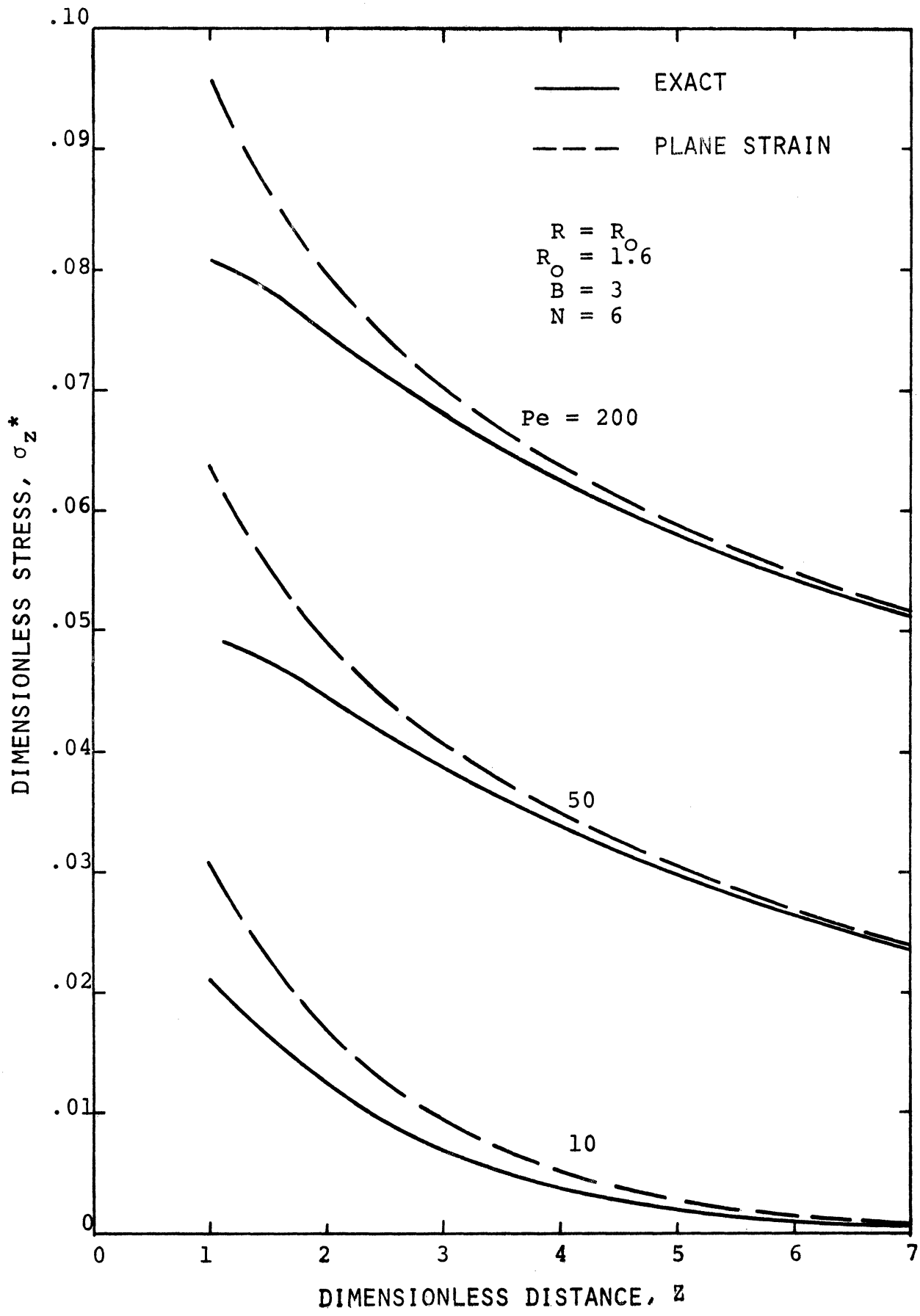

Figure 12. Effect of Peclet Number on Axial Stress. ($R = R_o$, $R_o = 1.6$, $B = 3$, $N = 6$)

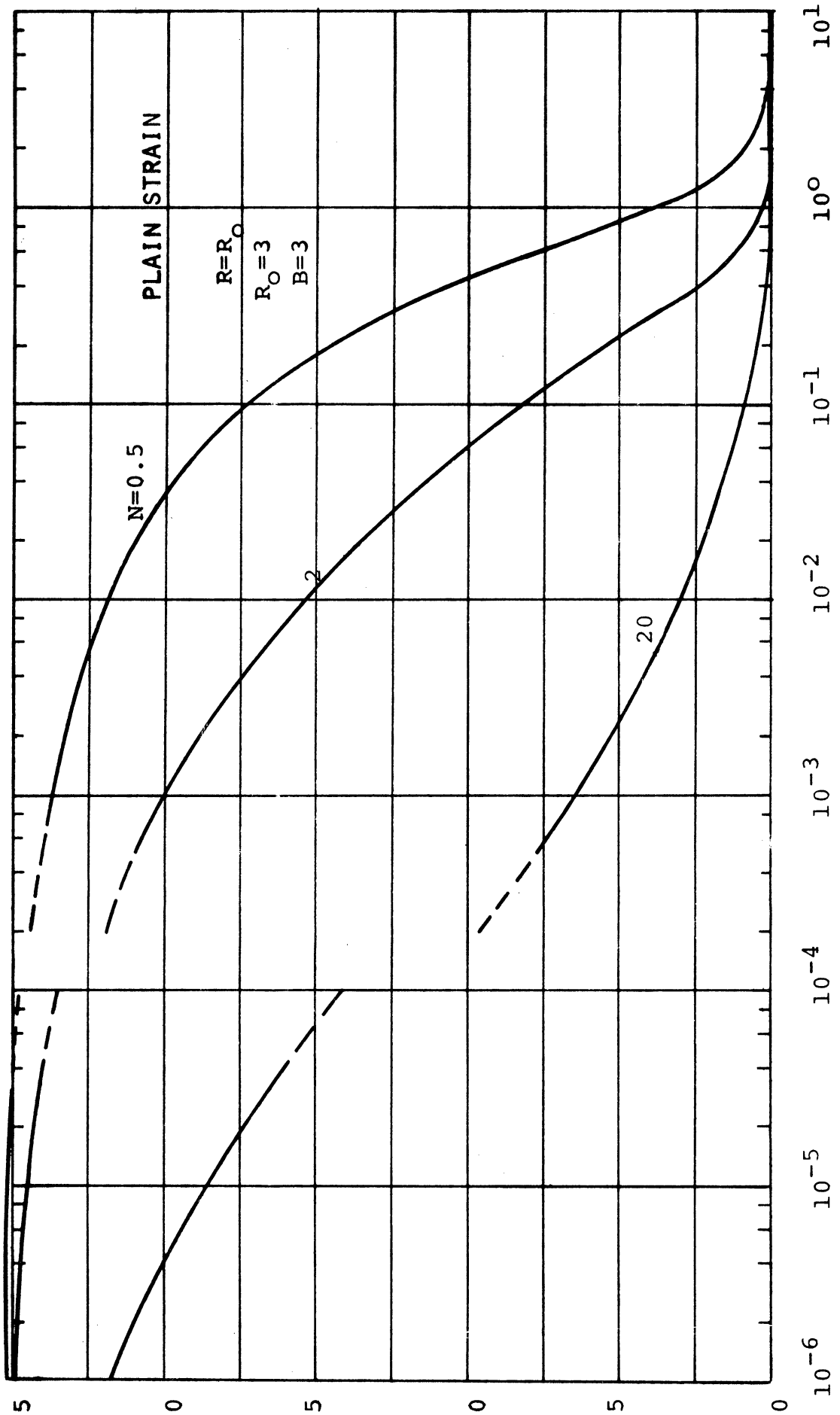

Figure 13. Effect of Modified Nusselt Number on Axial and Tangential Stress for Plane Strain. ($R = R_o$, $R_o = 3$, $B = 3$)

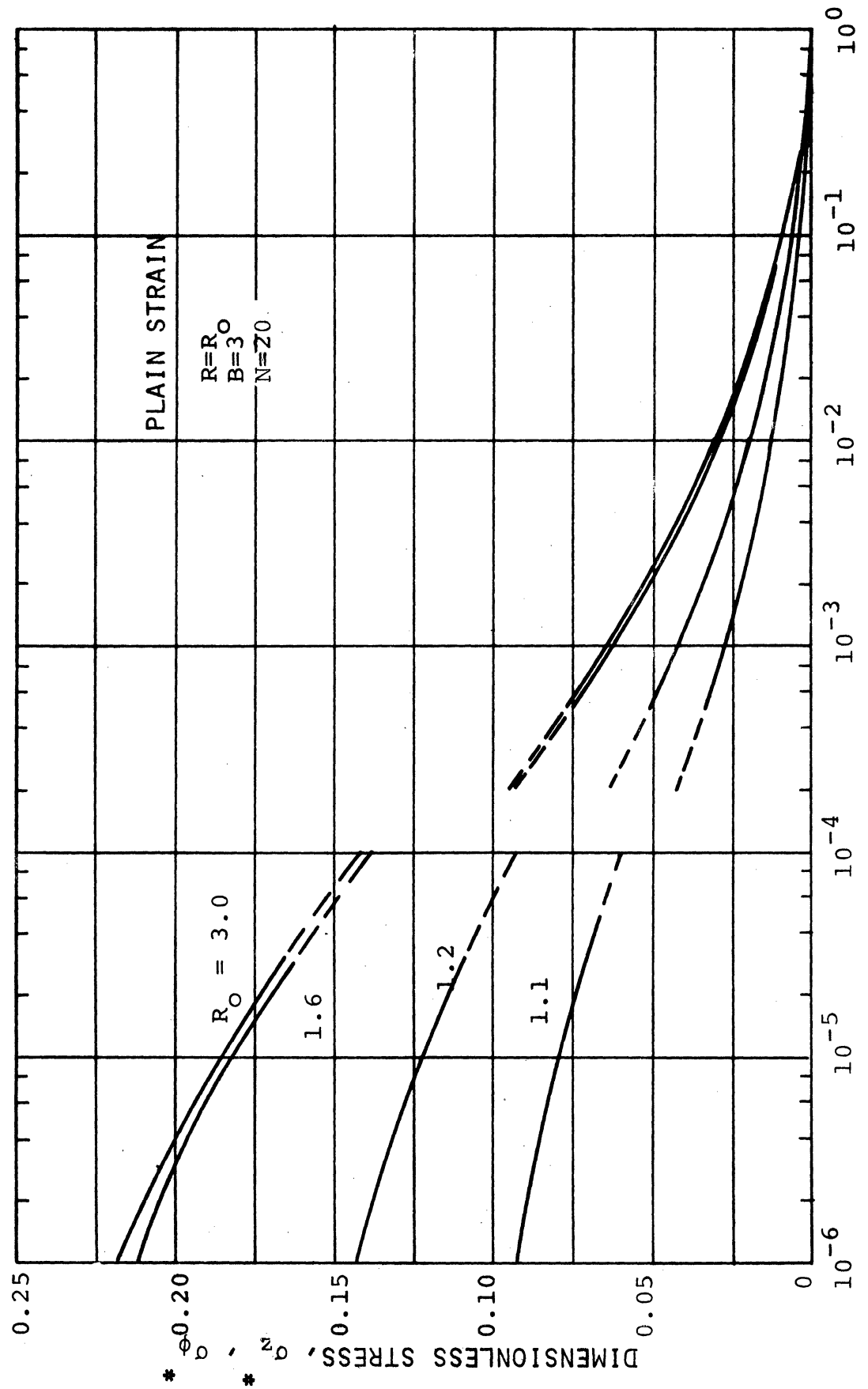

Figure 14. Effect of Tube Geometry on Axial and Tangential Stress for Plane Strain. ($R = R_o$, $B = 3$, $N = 20$)

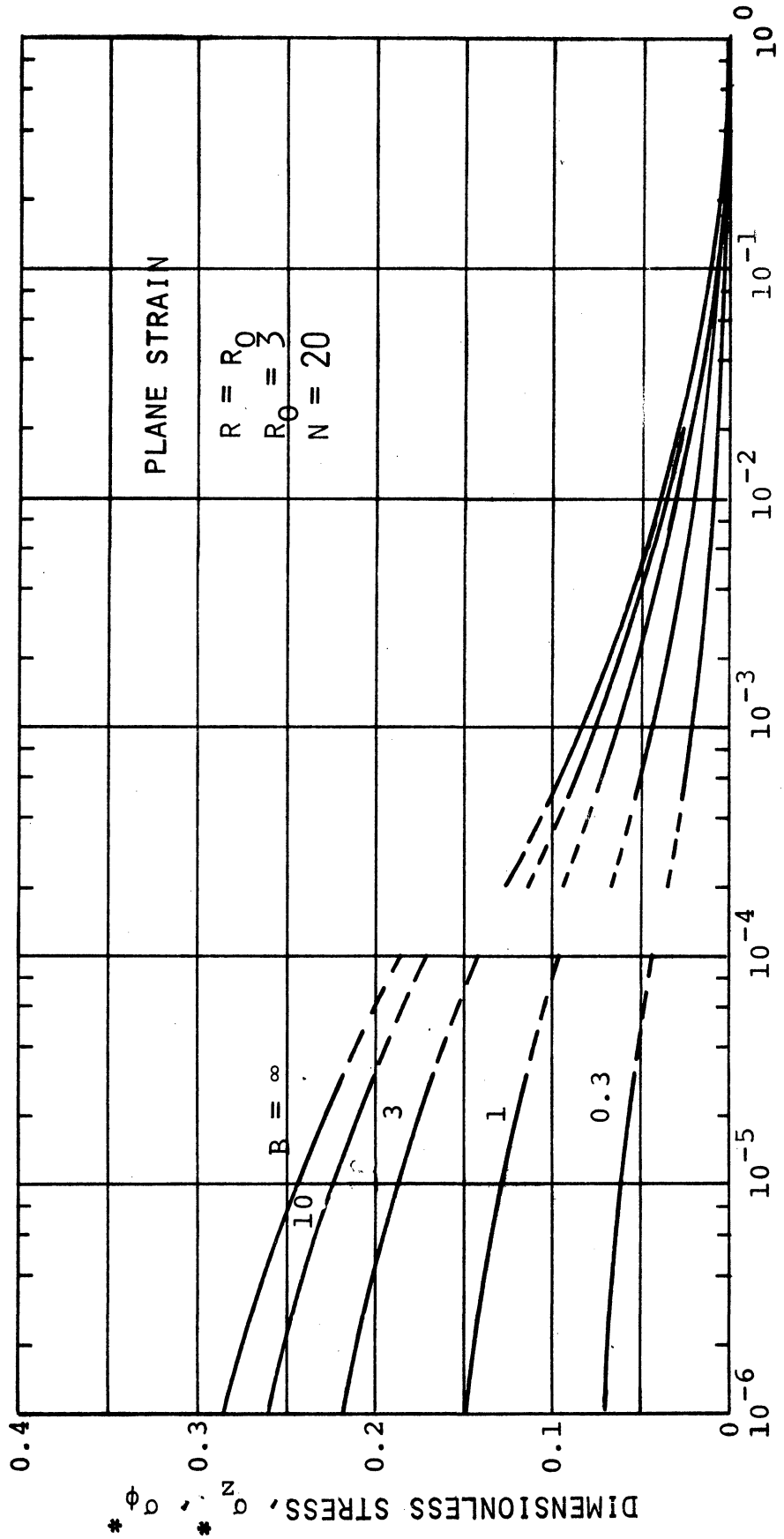

Figure 15. Effect of Modified Biot Number on Axial and Tangential Stress for Plane Strain. ($R = R_O$, $R_O = 3$, $N = 20$)

CHAPTER III

EXPERIMENTAL INVESTIGATION

A parallel flow tube and shell heat exchanger was constructed and experimental values of temperature and strain on the outside surface of the tube were obtained.

Hot and cold tap water was supplied to the tube and shell side of the heat exchanger, respectively. For the lower flow rates the hot water was supplied to the test section from a head tank.

A type 321 seamless stainless steel tube with .750 inch O.D. and .250 inch wall thickness was used as the test pipe. Two and one half feet of the tube extended upstream of the heat exchanger and served as the velocity development section. A schematic assembly drawing of the heat exchanger is shown in Figure 16. Figure 17 is a photograph of the test apparatus. At the upstream end of the heat exchanger the header chamber was silver soldered to the pipe. On the downstream side a sliding o-ring seal allowed free axial motion of the tube relative to the shell. Copper tubing with one inch I.D. and beginning 3/16 inches from the plastic insulator was used for the shell, giving a clearance of 1/8 inches in the annulus.

Temperature sensors and strain gages were mounted on the outside surface of the tube with high temperature cement and were installed at the axial locations indicated in Figure 16. The temperature sensors were of the nickel foil type (STG-50, Micro-Measurements, Inc.) and the strain gages were of the self temperature compensating foil type (MA-09-062AA-120, Micro-Measurements, Inc.). Lead wires of 30 gauge

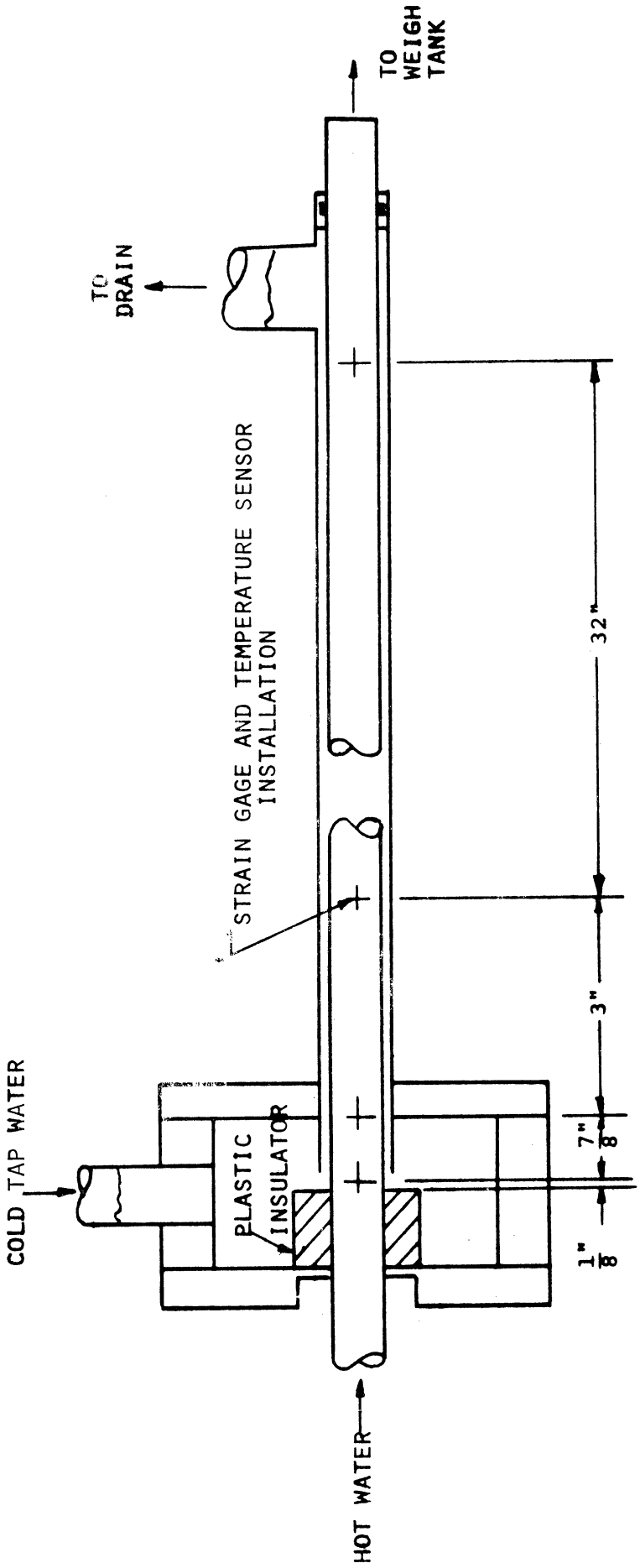

Figure 16. Schematic Assembly Drawing of Test Apparatus.

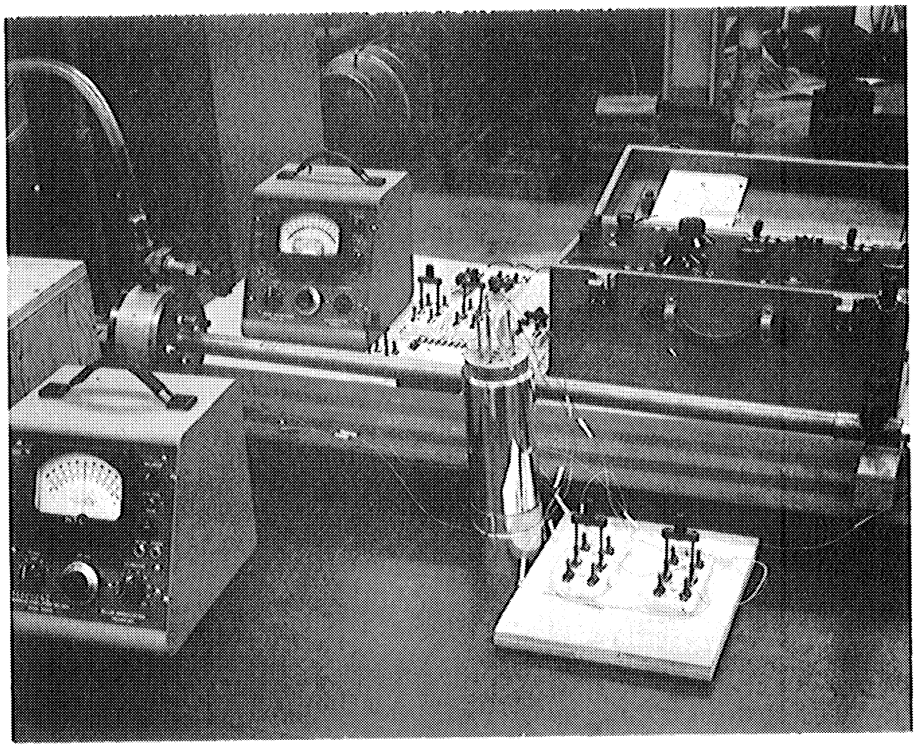

Figure 17. Photograph of Test Apparatus.

stranded copper, vinyl insulated cable were soldered to tabs cemented to the tube. Jumper wires formed from one strand of the lead wires were then soldered to the sensor and gage tabs. The lead wires were brought outside of the heat exchanger through two 16-wire Conax fittings mounted in the header chamber.

Because the installation was to be immersed in water the temperature sensors and strain gages had to be water proofed. Unfortunately application of a water-proofing compound insulates the surface to heat transfer and thus severe restrictions were placed on the choice of available materials. It was found that a coating of red Glyptal enamel over a coating of clear Glyptal varnish baked at the recommended temperature was satisfactory. In addition a thin coating of a rubber sealant was applied to the solder connections. The overall thickness of the water-proof coating and gage was less than .005 inches.

The temperature sensors were connected to an LST resistance network (LST-100-120, Vishay Instruments, Inc.). When used with an LST network the sensor-network circuit is equivalent to a half-bridge circuit with 120 ohm active and dummy arms. The output was measured on a model BAM-1 (Ellis Assoc.) bridge amplifier and meter.

The strain gages were wired into half-bridge circuits consisting of an active and a dummy gage. Dummy gages of the self temperature compensating foil type were mounted on a stainless steel plate and imbedded in vermiculite insulation to eliminate thermal effects due to convective currents in the air. Using the 3 wire method of wiring to eliminate thermal effects due to temperature variations in the lead wires the half-bridges were connected to a multi-channel switching and

balancing unit (Baldwin-Lima-Hamilton Corp.). The output was measured on a model BAM-1C (Ellis Assoc.) bridge amplifier and meter with which a sensitivity of 1 microinch per inch per division was obtainable.

At the beginning of the test series both the temperature sensors and strain gages were calibrated.

The inlet fluid temperatures were measured with 30 gauge copper-constantan thermocouples and a portable precision potentiometer (Model 8662, Leeds and Northrup Co.) was used to measure the E.M.F.

The mass flow rate was determined from measurements of mass and time obtained by use of a weigh tank and stopwatch.

Data were obtained for Reynolds numbers ranging from approximately 400 to 50,000 with points in the laminar, transition, and turbulent flow regimes. The Prandtl number was approximately equal to 3 for all runs. Figure 18 shows the variation of outside surface temperature with Peclet number at $z = 8$. It was found that the experimentally obtained temperatures were higher than predicted. The observed shift is attributed to the insulating effect of the sensor and water-proof coating. The experimental values of axial and tangential stress at $z = 8$ are shown in Figure 19. Natural convection effects apparently have influenced the results for the low laminar flow rates.

The uncertainty in the temperature measurement was less than $\pm$ 0.5°F and in the strain measurement less than $\pm$ 2 microin/in for the highest sensitivity used. Empirical correlations given by Kreith[9] were used to compute the heat transfer coefficient to the ambient.

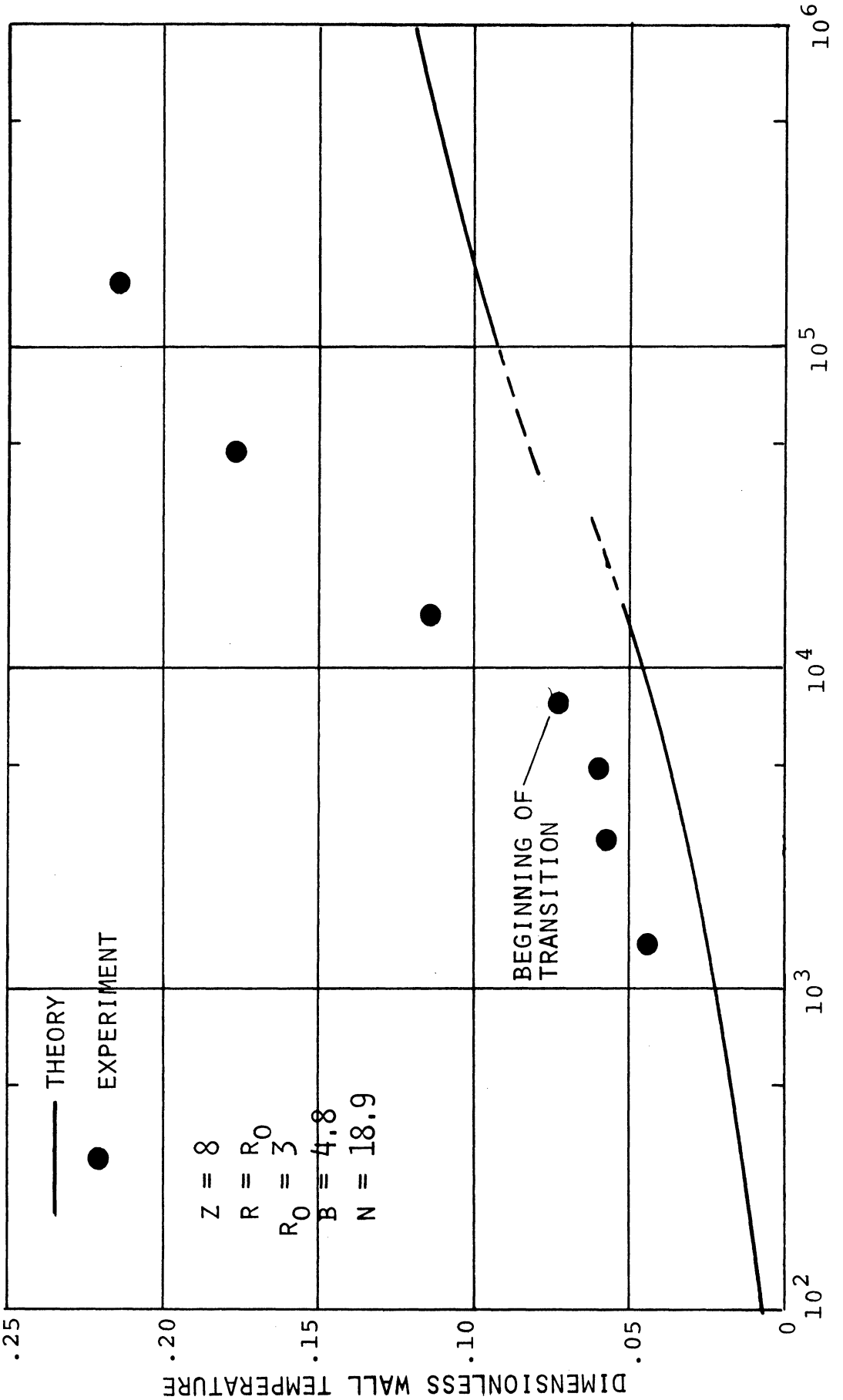

Figure 18. Experimental Temperature Data. (Z = 8, R = R_o, R_o = 3, B = 4.8, N = 18.9)

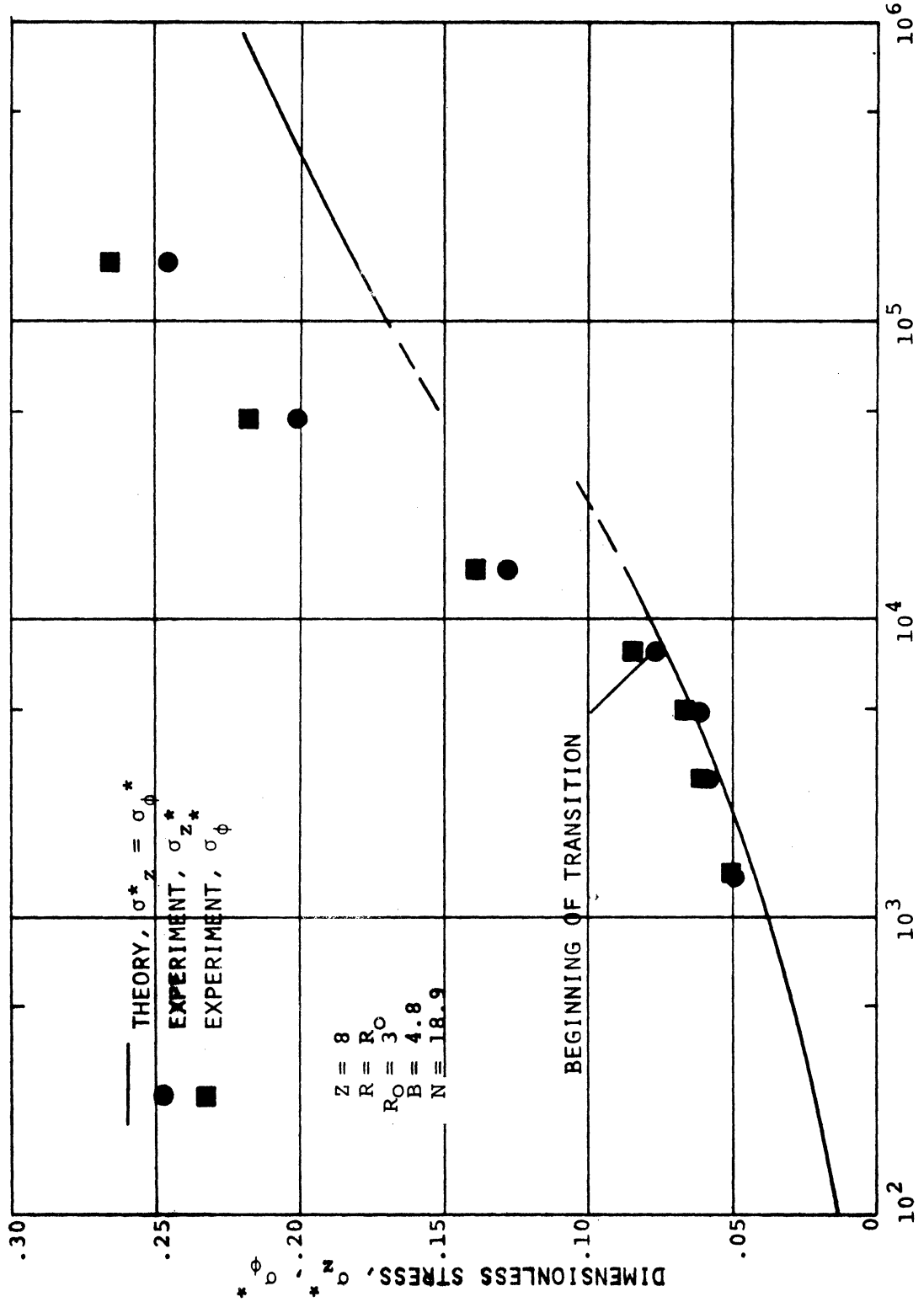

Figure 19. Experimental Axial and Tangential Stress Data. (Z = 8, R = R_O, R_O = 3, B = 4.8, N = 18.9)

CHAPTER IV

DISCUSSION OF RESULTS

Examination of the stress results shows that the behavior of the axisymmetric and plane strain stresses is qualitatively similar. The effect of the axial temperature gradient is confined to a region near the end of the tube where the gradient is largest. At axial distances greater than three outside tube radii, approximately, the plane strain solution may be used to obtain the stresses since the difference between the exact and plane strain result is small. Closer to the entrance the influence of the gradient may be important, depending on the values of the parameters.

It is noted that the axial temperature gradient decreases as the Peclet number increases, holding the other parameters constant. Since the asymptotic temperature solution is a large Peclet number solution for dimensionless distance of order one, the resulting stresses deviate little from the plane strain solution.

APPENDIX A

FORMULATION OF TEMPERATURE PROBLEM

A schematic of the physical model is given in Figure 20. The governing differential equations are obtained by applying the first law of thermodynamics to a system for the tube wall and to a control volume for the fluid. Under the assumptions made in Chapter II the governing equations are

$$\frac{\partial}{\partial r}\left(r \frac{\partial T}{\partial r}\right) = 0 \tag{A-1}$$

$$\rho_f C_f u^*(r) \frac{\partial T_f}{\partial z} = \frac{k_f}{r} \frac{\partial}{\partial r}\left(r \frac{\partial T_f}{\partial r}\right) \tag{A-2}$$

subject to the following boundary conditions

$$T(r_i, z) = T_f(r_i, z) \tag{A-3a}$$

$$-k \frac{\partial T}{\partial r}(r_o, z) = h\left[T(r_o, z) - T_\infty\right] \tag{A-3b}$$

$$T_f(r, 0) = T_o \tag{A-3c}$$

$$\frac{\partial T_f}{\partial r}(0, z) = 0 \tag{A-3d}$$

$$-k_f \frac{\partial T}{\partial r}(r_i, z) = \bar{h}\left[T_f(r_i, z) - T_\infty\right] \tag{A-3e}$$

where r and z denote the radial and axial coordinate, respectively, r_i the inside radius, r_o the outside radius, T the wall temperature, T_f the fluid temperature, T_∞ the ambient temperature, T_o the inlet temperature, ρ_f the fluid mass density, C_f the fluid specific heat, $u^*(r)$ the fluid velocity, k and k_f the thermal conductivity of the wall and fluid, respectively, h the heat transfer coefficient to

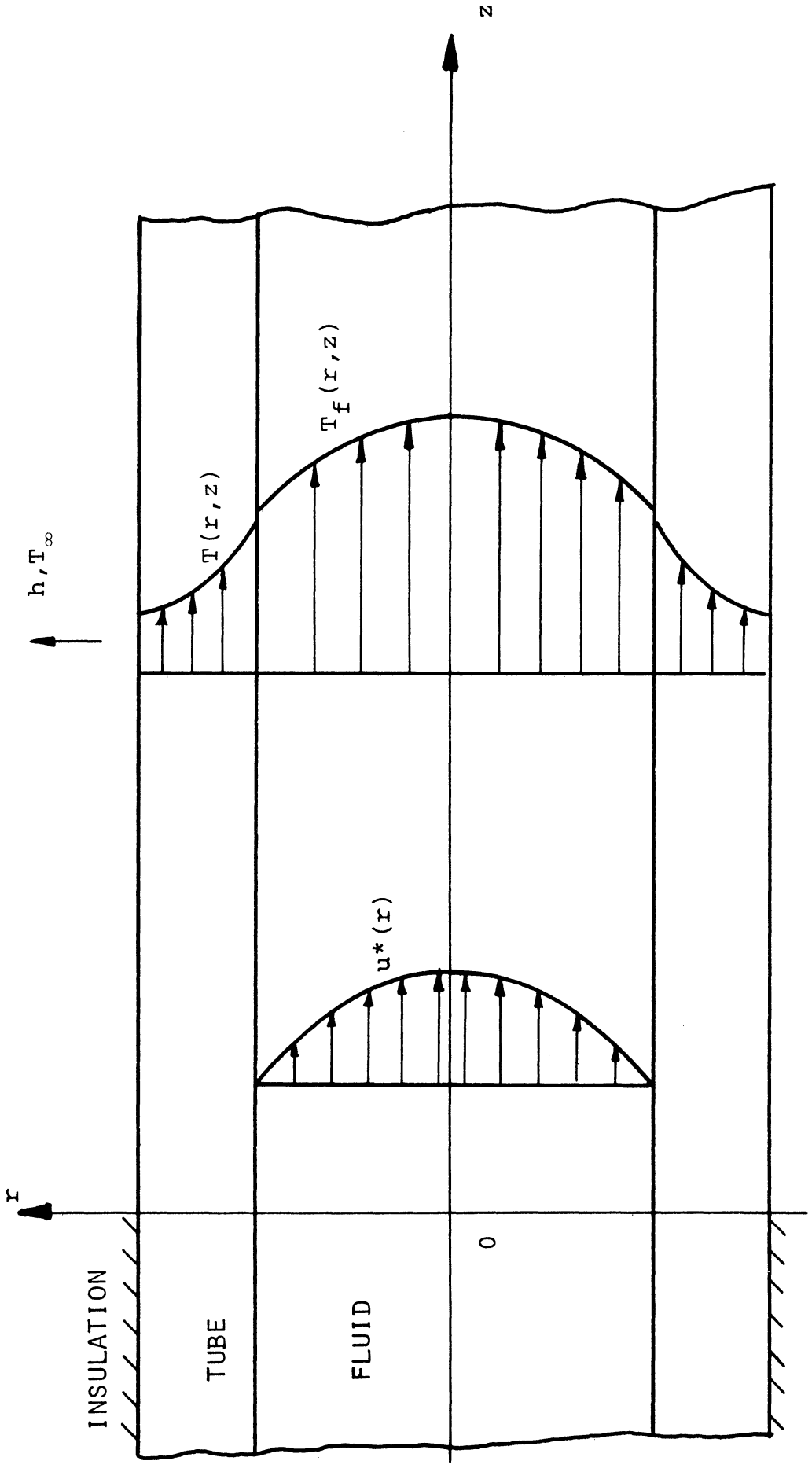

Figure 20. Schematic of Modified Graetz Model.

ambient, and $\bar{h} = 1/r_o\left[\frac{1}{r_o h} + \frac{1}{k}\ln\frac{r_o}{r_i}\right]$ the overall heat transfer coefficient.

The fully developed velocity distribution in laminar flow is given by

$$u^*(r) = 2U\left[1 - \left(\frac{r}{r_i}\right)^2\right] \tag{A-4}$$

where U denotes the average velocity. Substitution of Equation (A-4) into Equation (A-2) yields

$$2\rho_f C_f U\left[1-\left(\frac{r}{r_i}\right)^2\right]\frac{\partial T_f}{\partial z} = \frac{k_f}{r}\frac{\partial}{\partial r}\left(r\frac{\partial T_f}{\partial r}\right) \tag{A-5}$$

Finally, rearrangement of the formulation into dimensionless form gives

$$\frac{\partial}{\partial R}\left(R\frac{\partial \phi}{\partial R}\right) = 0 \tag{A-6}$$

$$Pe\,(1-R^2)\frac{\partial \theta}{\partial z} = \frac{1}{R}\frac{\partial}{\partial R}\left(R\frac{\partial \theta}{\partial R}\right) \tag{A-7}$$

subject to

$$\phi(1,z) = \theta(1,z) \tag{A-8a}$$

$$\frac{\partial \phi}{\partial R}(R_o,z) = -\frac{B}{R_o}\phi(R_o,z) \tag{A-8b}$$

$$\theta(R,0) = 1 \tag{A-8c}$$

$$\frac{\partial \theta}{\partial R}(0,z) = 0 \tag{A-8d}$$

$$\frac{\partial \theta}{\partial R}(1,z) = -N\,\theta(1,z) \tag{A-8e}$$

where the dimensionless variables and parameters are defined by

$$R = \frac{r}{r_i} \quad , \quad R_o = \frac{r_o}{r_i} \quad , \quad z = \frac{z}{r_i} \quad , \quad B = \frac{h r_o}{k}$$

$$\phi = \frac{T - T_\infty}{T_o - T_\infty} \quad , \quad \theta = \frac{T_f - T_\infty}{T_o - T_\infty} \quad , \quad P_e = \frac{2 r_i U \rho_f C_f}{K_f}$$

$$N = \frac{\frac{h r_o}{k_f}}{\left[1 + \left(\frac{h r_o}{k} \right) \ln \frac{r_o}{r_i} \right]}$$

The parameter P_e is the well known Peclet number (Reynolds number times Prandtl number) based on diameter, B is a modified Biot modulus, and N is a modified Nusselt number.

APPENDIX B

APPROXIMATE TEMPERATURE FORMULATION FOR THE ENTRANCE REGION

A schematic of the physical model is shown in Figure 21. The assumptions applying to the formulation are:

1) The physical properties are constant.
2) The velocity gradient in the fluid is constant and equal to the velocity gradient at the wall of a circular tube with hydrodynamically developed laminar flow.
3) Axial conduction is negligible.
4) The heat transfer coefficient to the ambient is constant.
5) The fluid is incompressible.

The governing equation is found by applying the first law of thermodynamics to a fluid control volume and is given by

$$\rho_f c_f u^*(\xi) \frac{\partial T_f}{\partial z} = k_f \frac{\partial^2 T_f}{\partial \xi^2} \tag{B-1}$$

subject to

$$T_f(\xi, 0) = T_0 \tag{B-2a}$$

$$T_f(\infty, z) = T_0 \tag{B-2b}$$

$$k_f \frac{\partial T_f}{\partial \xi}(0, z) = \bar{h}\,[T_f(0, z) - T_\infty] \tag{B-2c}$$

where ξ and z denote the transverse and longitudinal coordinate, respectively, T_f the fluid temperature, T_0 the undisturbed fluid temperature, T_∞ the ambient temperature, $\bar{h}$ the overall heat transfer coefficient defined in Appendix A, ρ_f the mass density, c_f the

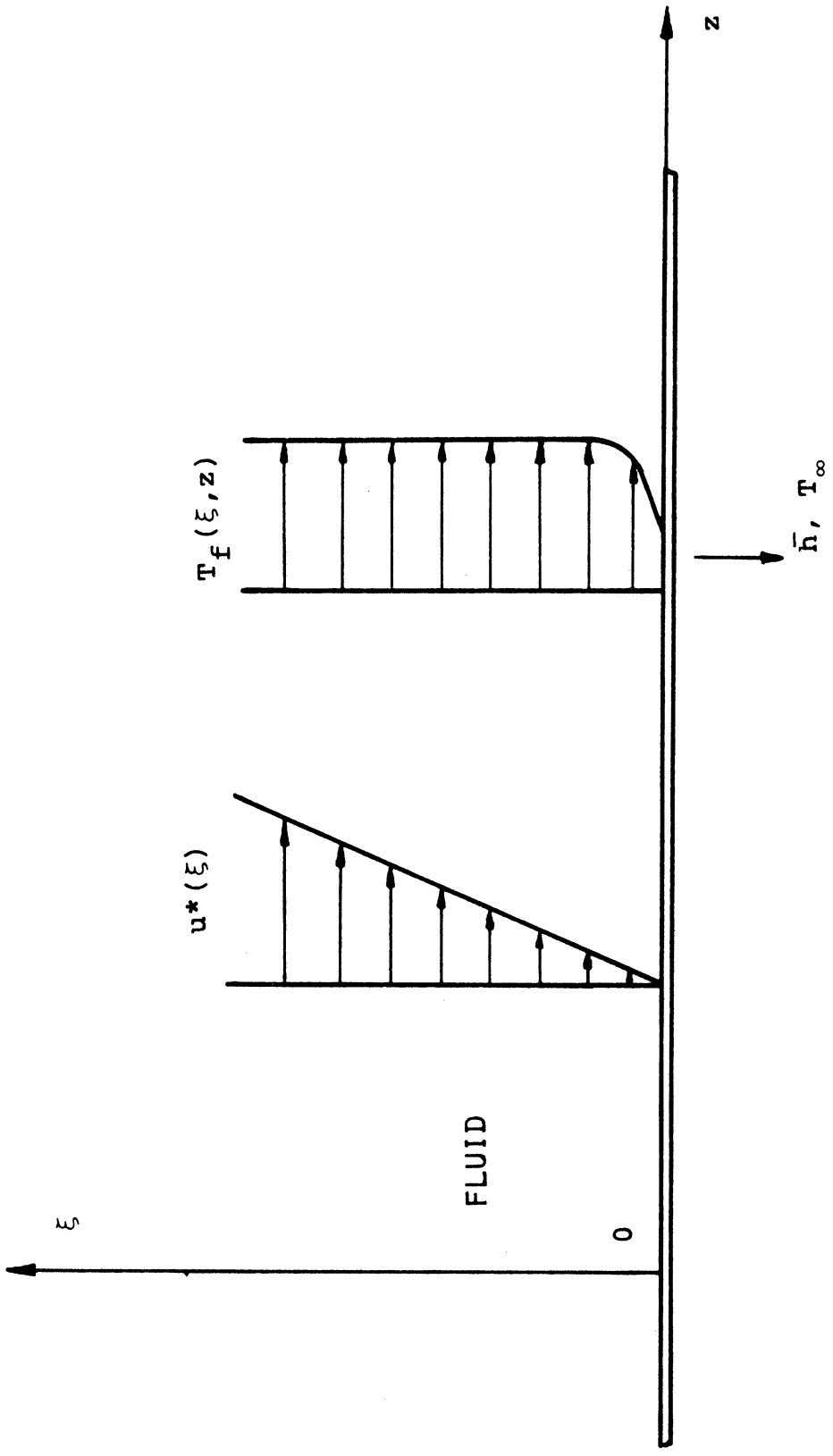

Figure 21. Schematic of Modified Leveque Model.

specific heat, k_f the thermal conductivity, and $u^*(\xi)$ the local fluid velocity.

The velocity distribution is

$$u^*(\xi) = \frac{4U}{r_i}\,\xi \tag{B-3}$$

where U is the average velocity in the tube and r_i the inside radius. Substitution of Equation (B-3) into Equation (B-1) yields

$$\frac{4\rho_f C_f U}{r_i}\,\xi\,\frac{\partial T_f}{\partial z} = k_f\,\frac{\partial^2 T_f}{\partial \xi^2} \tag{B-4}$$

Finally, rearrangement of the formulation into dimensionless form gives

$$y\,\frac{\partial \theta}{\partial \bar{z}} = \frac{\partial^2 \theta}{\partial y^2} \tag{B-5}$$

subject to

$$\theta(y,0) = 0 \tag{B-6a}$$

$$\theta(\infty,\bar{z}) = 0 \tag{B-6b}$$

$$\frac{\partial \theta}{\partial y}(0,\bar{z}) = N\left[\theta(0,\bar{z}) - 1\right] \tag{B-6c}$$

where

$$\theta = \frac{T_f - T_0}{T_\infty - T_0}\,, \quad y = \frac{\xi}{r_i}\,, \quad \bar{z} = \frac{z}{r_i}\,\frac{1}{2Pe}\,, \tag{B-7}$$

$$Pe = \frac{2r_i U \rho_f C_f}{k_f}\,, \qquad N = \frac{\frac{h r_o}{k_f}}{\left[1 + \left(\frac{h r_o}{k}\right) \ln \frac{r_o}{r_i}\right]}$$

and Pe and N are the Peclet number and modified Nusselt number defined previously in Appendix A.

APPENDIX C

EFFECT OF AXIAL CONDUCTION IN THE TUBE WALL

The effect is studied in the end section of a flat plate for two cases as shown in Figure 22. In case 1, which was solved by Arpaci,[2] an exponential axial temperature distribution is maintained on one boundary while the other boundary is maintained at zero temperature. In case 2 both boundaries have the same exponentially decreasing temperature distribution. The axial effect at the end is shown as γ in Figure 22.

Using the variational procedure the temperature profile in the wall for case 1 is assumed to be

$$\theta_1 = \eta e^{-\mu\xi} - 4\gamma\eta(1-\eta)\,X(\xi) \qquad \text{(C-1)}$$

where θ_1 is the dimensionless wall temperature, η and ξ the dimensionless transverse and axial coordinate, respectively, μ a constant, $X(\xi)$ an unknown function of ξ to be determined, and γ is a parameter which satisfies $\gamma < \frac{1}{4}$. This restriction on γ is required in order that the approximate profile does not violate the physics and is determined by the end conditions, e.g. end fittings on pipe.

The variational formulation is given by

$$\int_0^1\int_0^\infty \left(\frac{\partial^2\theta_1}{\partial\xi^2} + \frac{\partial^2\theta_1}{\partial\eta^2}\right)\delta\theta_1\, d\eta\, d\xi = 0 \qquad \text{(C-2)}$$

Substitution of Equation (C-1) into Equation (C-2) and integration over the interval 0 - 1 of η yields

$$\int_0^\infty \left[\frac{\mu^2}{12}e^{-\mu\xi} - \frac{4\gamma}{30}X''(\xi) + \frac{4\gamma}{3}X(\xi)\right]\delta X\, d\xi = 0 \qquad \text{(C-3)}$$

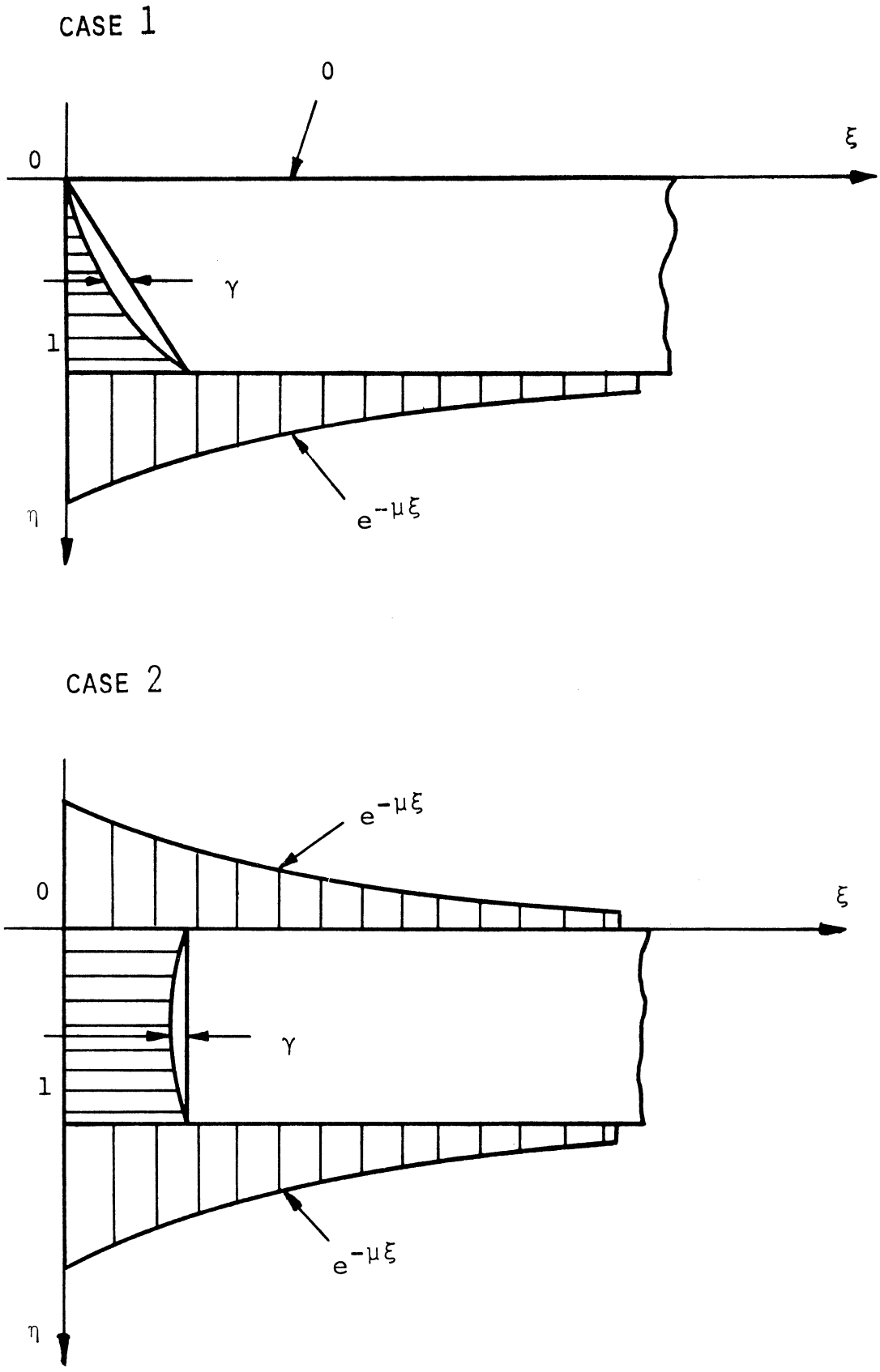

Figure 22. Schematic of Physical Models Used in Determining Effect of Axial Conduction.

Upon equating the integrand to zero and rearranging one finds

$$X'' - 10X = \frac{5}{8\gamma}\mu^2 e^{-\mu\xi} \tag{C-4}$$

where the boundary conditions are

$$X(0) = 1, \quad X(\infty) = 0 \tag{C-5}$$

The solution of Equation (C-4) being elementary is written immediately as

$$X = \frac{5\mu^2}{8\gamma(\mu^2-10)} e^{-\mu\xi} + \left(1 - \frac{5\mu^2}{8\gamma(\mu^2-10)}\right) e^{-\sqrt{10}\,\xi} \tag{C-6}$$

Finally, substitution of Equation (C-6) into Equation (C-1) yields

$$\theta_1 = \eta e^{-\mu\xi} - \eta(1-\eta)\left[4\gamma e^{-\sqrt{10}\,\xi} + \frac{5\mu^2}{2(\mu^2-10)}\left(e^{-\mu\xi} - e^{-\sqrt{10}\,\xi}\right)\right] \tag{C-7}$$

For case 2 the temperature profile is assumed to be

$$\theta_2 = e^{-\mu\xi} - 4\gamma\eta(1-\eta)X(\xi) \tag{C-8}$$

where the previous restriction on γ is not required. Following the same procedure as for case 1 but omitting the intermediate details one obtains

$$\theta_2 = e^{-\mu\xi} - \eta(1-\eta)\left[4\gamma e^{-\sqrt{10}\,\xi} + \frac{5\mu^2}{(\mu^2-10)}\left(e^{-\mu\xi} - e^{-\sqrt{10}\,\xi}\right)\right] \tag{C-9}$$

Numerical results for $\eta = \frac{1}{2}$ are tabulated in Tables 1C and 2C for case 1 and case 2, respectively, where θ_1 and θ_2 denote the temperature including axial conduction, θ_1^* and θ_2^* denote the temperature neglecting axial conduction, and Δ_1 and Δ_2 denote the percent deviation of the temperature including axial conduction from the

TABLE 1C

EFFECT OF AXIAL CONDUCTION FOR CASE 1

ζ	$\mu = 0.269$			$\mu = 0.400$			$\mu = 0.680$		
	θ_1	θ_1^*	Δ_1	θ_1	θ_1^*	Δ_1	θ_1	θ_1^*	Δ_1
0.5	.414	.437	-5.19	.390	.409	-4.76	.346	.356	-2.92
1.0	.380	.382	- .52	.336	.335	.33	.262	.253	3.47
1.5	.336	.334	.57	.279	.274	1.60	.190	.180	5.31
2.0	.294	.292	.83	.229	.225	1.92	.136	.128	5.84
2.5	.257	.255	.89	.188	.184	2.01	.097	.091	6.00
3.0	.225	.223	.91	.154	.151	2.03	.069	.065	6.04
4.0	.172	.170	.91	.103	.101	2.03	.035	.033	6.06
5.0	.131	.130	.91	.069	.068	2.03	.018	.017	6.06

TABLE 2C

EFFECT OF AXIAL CONDUCTION FOR CASE 2

ζ	$\mu = 0.269$			$\mu = 0.400$			$\mu = 0.680$		
	θ_2	θ_2^*	Δ_2	θ_2	θ_2^*	Δ_2	θ_2	θ_2^*	Δ_2
0.5	.855	.874	-2.25	.805	.819	-1.62	.717	.712	.70
1.0	.765	.764	0.17	.678	.670	1.11	.529	.507	4.51
1.5	.673	.668	.74	.559	.549	1.80	.380	.361	5.61
2.0	.589	.584	.87	.458	.449	1.97	.272	.257	5.93
2.5	.515	.510	.90	.375	.368	2.02	.194	.183	6.02
3.0	.450	.446	.91	.307	.301	2.03	.138	.130	6.05
4.0	.344	.341	.91	.206	.202	2.03	.070	.066	6.06
5.0	.263	.261	.91	.138	.135	2.03	.035	.033	6.06

temperature neglecting axial conduction. The values μ = 0.269, 0.400, and 0.680 correspond to the wall temperature solution for N = 1, 2, and 20, respectively, when $P_e = 10$. A typical value of $\gamma = \frac{1}{8}$ was used in the calculations.

Examination of the results shows that the effect of axial conduction in the end region due to end conditions decays rapidly and is small at $\zeta = 2$. The effect due to the imposed axial gradient on the surface produces a constant percentage deviation from the solution neglecting axial conduction when $\zeta \geq 4$. The magnitude of this deviation increases with μ since the axial gradient increases with μ . However, for significant stresses beyond $\zeta = 2$ the value of μ must be less than 1, approximately. Therefore, it is concluded that the effect of axial conduction is small for $\zeta > 2$ and may be neglected.

APPENDIX D

TABULATED VALUES OF THE EIGENVALUES, EIGENFUNCTIONS AT THE WALL, AND COEFFICIENTS FOR THE MODIFIED GRAETZ SOLUTION

TABLE 1D

EIGENVALUES, EIGENFUNCTIONS AT THE WALL,
AND COEFFICIENTS FOR N = 20

n	λ_n	A_n	$R_n(1)$	B_n
0	2.6069	1.4573	.0494	0.0719
1	6.5099	- .7628	-.0632	.0482
2	10.450	.5382	.0712	.0383
3	14.403	- .4217	-.0768	.0324
4	18.363	.3489	.0808	.0282
5	22.328	- .2985	-.0840	.0251
6	26.297	.2612	.0865	.0226
7	30.269	- .2323	-.0885	.0206
8	34.244	.2093	.0901	.0189
9	38.220	- .1904	-.0915	.0174
10	42.198	.1747	.0926	.0162
11	46.178	- .1613	-.0936	.0151
12	50.159	.1498	.0943	.0141
13	54.142	- .1397	-.0950	.0133
14	58.125	.1309	.0955	.0125
15	62.109	- .1231	-.0959	.0118
16	66.094	.1161	.0963	.0112
17	70.080	- .1099	-.0966	.0106
18	74.067	.1042	.0968	.0101
19	78.054	- .0991	-.0970	.0096

TABLE 2D

EIGENVALUES, EIGENFUNCTIONS AT THE WALL,
AND COEFFICIENTS FOR N = 17

m	λ_m	A_m	$R_m(1)$	B_m
0	2.5905	1.4538	.0578	.0840
1	6.4826	- .7549	-.0734	.0554
2	10.415	.5290	.0822	.0435
3	14.363	- .4121	-.0881	.0363
4	18.319	.3392	.0923	.0313
5	22.281	- .2887	-.0955	.0276
6	26.247	.2516	.0979	.0246
7	30.217	- .2229	-.0998	.0222
8	34.189	.2000	.1012	.0203
9	38.164	- .1814	-.1024	.0186
10	42.141	.1658	.1033	.0171
11	46.120	- .1526	-.1040	.0159
12	50.100	.1413	.1046	.0148
13	54.082	- .1315	-.1050	.0138
14	58.065	.1229	.1054	.0129
15	62.049	- .1153	-.1056	.0122
16	66.033	.1085	.1057	.0115
17	70.019	- .1024	-.1058	.0108
18	74.006	.0970	.1059	.0103
19	77.993	- .0920	-.1059	.0097

TABLE 3D

EIGENVALUES, EIGENFUNCTIONS AT THE WALL,
AND COEFFICIENTS FOR N = 6

m	λ_m	A_m	$R_m(1)$	B_m
0	2.4072	1.4092	.1530	.2157
1	6.2036	-.6589	-.1767	.1164
2	10.087	.4262	.1835	.0782
3	14.006	-.3112	-.1849	.0575
4	17.945	.2428	.1840	.0447
5	21.897	-.1975	-.1822	.0360
6	25.857	.1655	.1799	.0298
7	29.824	-.1417	-.1774	.0251
8	33.796	.1234	.1749	.0216
9	37.772	-.1089	-.1724	.0188
10	41.751	.0972	.1700	.0165
11	45.732	-.0876	-.1676	.0147
12	49.716	.0795	.1654	.0132
13	53.701	-.0727	-.1632	.0119
14	57.687	.0668	.1611	.0108
15	61.675	-.0617	-.1592	.0098
16	65.664	.0573	.1573	.0090
17	69.653	-.0534	-.1554	.0083
18	73.644	.0500	.1537	.0077
19	77.635	-.0469	-.1520	.0071

TABLE 4D

EIGENVALUES, EIGENFUNCTIONS AT THE WALL,
AND COEFFICIENTS FOR N = 2.

m	λ_m	A_m	$R_m(1)$	B_m
0	2.0000	1.2961	.3679	.4768
1	5.7439	-.4471	-.3328	.1488
2	9.6451	.2467	.3027	.0747
3	13.590	-.1635	-.2807	.0459
4	17.555	.1194	.2640	.0315
5	21.530	-.0926	-.2506	.0232
6	25.511	.0748	.2396	.0179
7	29.496	-.0623	-.2304	.0143
8	33.484	.0530	.2224	.0118
9	37.474	-.0459	-.2155	.0099
10	41.465	.0403	.2093	.0084
11	45.458	-.0358	-.2039	.0073
12	49.451	.0321	.1989	.0064
13	53.446	-.0291	-.1944	.0057
14	57.441	.0265	.1903	.0050
15	61.437	-.0243	-.1866	.0045
16	65.433	.0224	.1831	.0041
17	69.429	-.0207	-.1799	.0037
18	73.426	.0193	.1769	.0034
19	77.423	-.0180	-.1740	.0031

TABLE 5D

EIGENVALUES, EIGENFUNCTIONS AT THE WALL,
AND COEFFICIENTS FOR N = 1

n	λ_n	A_n	$R_n(1)$	B_n
0	1.6413	1.2013	.5497	.6603
1	5.4783	-.2929	-.4079	.1195
2	9.4360	.1467	.3484	.0511
3	13.415	-.0930	-.3133	.0291
4	17.403	.0663	.2892	.0192
5	21.394	-.0506	-.2711	.0137
6	25.388	.0404	.2569	.0104
7	29.383	-.0333	-.2453	.0082
8	33.379	.0282	.2355	.0066
9	37.376	-.0243	-.2272	.0055
10	41.373	.0212	.2199	.0047
11	45.371	-.0188	-.2135	.0040
12	49.369	.0168	.2077	.0035
13	53.367	-.0152	-.2026	.0031
14	57.366	.0138	.1979	.0027
15	61.364	-.0126	-.1937	.0024
16	65.363	.0116	.1897	.0022
17	69.362	-.0107	-.1861	.0020
18	73.361	.0100	.1828	.0018
19	77.360	-.0093	-.1796	.0017

TABLE 6D

EIGENVALUES, EIGENFUNCTIONS AT THE WALL,
AND COEFFICIENTS FOR N = 0.5

m	λ_m	A_m	$R_m(1)$	B_m
0	1.2716	1.1204	.7169	0.8032
1	5.2951	-.1710	-.4509	.0771
2	9.3063	.0802	.3725	.0299
3	13.312	-.0496	-.3299	.0164
4	17.316	.0349	.3018	.0105
5	21.318	-.0264	-.2813	.0074
6	25.320	.0210	.2655	.0056
7	29.321	-.0172	-.2527	.0044
8	33.322	.0145	.2420	.0035
9	37.323	-.0125	-.2329	.0029
10	41.324	.0109	.2251	.0025
11	45.324	-.0096	-.2182	.0021
12	49.325	.0086	.2121	.0018
13	53.325	-.0077	-.2066	.0016
14	57.326	.0070	.2017	.0014
15	61.326	-.0064	-.1971	.0013
16	65.326	.0059	.1930	.0011
17	69.327	-.0055	-.1892	.0010
18	73.327	.0051	.1857	.0009
19	77.327	-.0047	-.1824	.0009

APPENDIX E

THERMAL STRESS SOLUTION FOR PLANE STRAIN

For the circular cylindrical geometry the plane strain analysis gives the stress distribution produced by radially distributed but axially and circumferentially uniform temperature distributions. However, it has been demonstrated that for "sufficiently smooth" temperature variations in the axial direction the one dimensional approximation will yield accurate results. (See for instance, Boley and Weiner[3]) The axisymmetric temperature expression is used in the plane strain solution and the axial dependence is carried as a parameter.

Because the plane strain solution for thermal stresses in circular cylinders is well known and can be found in most text books on thermal stresses, e.g. Boley and Weiner,[3] the solution is given without further discussion as

$$\sigma_r^* = \frac{1}{R^2}\left[\frac{R^2-1}{R_o^2-1}\int_1^{R_o}\phi(R,z)\,R\,dR - \int_1^{R}\phi(R,z)\,R\,dR\right] \qquad (D\text{-}1)$$

$$\sigma_\varphi^* = \frac{1}{R^2}\left[\frac{R^2+1}{R_o^2-1}\int_1^{R_o}\phi(R,z)\,R\,dR + \int_1^{R}\phi(R,z)R\,dR - \phi(R,z)R^2\right] \qquad (D\text{-}2)$$

When the end faces are free of external constraints the axial stress can be written in terms of σ_r^* and σ_φ^* and is given by

$$\sigma_z^* = \sigma_r^* + \sigma_\varphi^* \qquad (D\text{-}3)$$

The shear stresses along coordinate directions are zero.

The wall temperature distribution is represented by

$$\phi(R,z) = (1 - \overline{B}\ln R)\,g(z) \qquad (D\text{-}4)$$

where $g(z)$ is an arbitrary function of z. Substitution of Equation (D-4) into Equation (D-1) and (D-2) yields

$$\sigma_r^* = \frac{g(z)}{R^2}\left[\frac{R^2-1}{R_o^2-1}\left\{\tfrac{1}{2}[R_o^2-1] - \overline{B}\left(\tfrac{1}{2}R_o^2 \ln R_o - \tfrac{1}{4}[R_o^2-1]\right)\right\}\right.$$

$$\left. -\left\{\tfrac{1}{2}(R^2-1) - \overline{B}\left(\tfrac{1}{2}R^2 \ln R - \tfrac{1}{4}[R^2-1]\right)\right\}\right] \qquad \text{(D-5)}$$

and

$$\sigma_\phi^* = \frac{g(z)}{R^2}\left[\frac{R^2+1}{R_o^2-1}\left\{\tfrac{1}{2}[R_o^2-1] - \overline{B}\left(\tfrac{1}{2}R_o^2 \ln R_o - \tfrac{1}{4}[R_o^2-1]\right)\right\}\right.$$

$$\left. +\left\{\tfrac{1}{2}[R^2-1] - \overline{B}\left(\tfrac{1}{2}R^2 \ln R - \tfrac{1}{4}[R^2-1]\right)\right\} - \left\{1-\overline{B}\ln R\right\}R^2\right] \qquad \text{(D-6)}$$

When considering the exact temperature solution

$$g(z) = \sum_{m=0}^{\infty} B_m e^{-\mu_m z} \qquad \text{(D-7)}$$

and for the entrance region approximation

$$g(z) = 1 + \sum_{m=1}^{\infty} \frac{(-1)^m (C z^{1/3})^m}{\Gamma(1+\frac{m}{3})} \qquad \text{(D-8)}$$

BIBLIOGRAPHY

1. Arpaci, V. S. Conduction Heat Transfer. Addison-Wesley, 1966.

2. Arpaci, V. S. Class Notes on "Thermoelasticity". University of Michigan, 1965.

3. Boley, B. A., and Weiner, J. H. Theory of Thermal Stresses. John Wiley and Sons, 1960.

4. Boussinesq, J. "Application des Potentiels a l'Etude de l'Equilibre et du Movement des Solides Elastiques." Gauthiers-Villars, Paris, 1885.

5. Galerkin, B. "Contribution a la Solution Generale du Probleme de la Theorie de l'Elasticite dans le cas de Trois Dimensions." Compt. Rend., 190 (1930), 1047.

6. Goodier, J. N. "On the Integration of the Thermo-Elastic Equations." Phil. Mag., 23 (1937), 1017.

7. Jakob, M. Heat Transfer I. John Wiley and Sons, 1949.

8. Knudsen, J. G. and Katz, D. L. Fluid Dynamics and Heat Transfer. McGraw-Hill, 1958.

9. Kreith, F. Principles of Heat Transfer. 2nd Ed., International, 1965.

10. Love, A. E. H. Mathematical Theory of Elasticity. 4th Ed., Dover, (1944), 274.

11. Nowacki, W. Thermoelasticity. Addison-Wesley, 1960.

12. Papkovich, P. F. "Solution Generale des Equations Differentielles, Fondamentales d'Elasticite, Exprimee par Trois Functions Harmoniques." Compt. Rend., 195 (1932), 513.

13. Parkus, H. Instationare Warmespannungen. Springer-Verlag, 1959.

14. Parkus, H. "Thermal Stresses in Pipes." J. App. Mech., 75 (1953), 485.

15. Schenk, J. and Dumore, J. M. "Heat Transfer in Laminar Flow Through Cylindrical Tubes." App. Sci. Res., 4A (1953), 39.

16. Schneider, P. J. "Effect of Axial Fluid Conduction on Heat Transfer in the Entrance Regions of Parallel Plates and Tubes." Heat Transfer and Fluid Mechanics Institute, (Preprints of papers) (1956), 41.

17. Van Wylen, G. J. and Sonntag, R. E. Fundamentals of Classical Thermodynamics. John Wiley and Sons, 1965.

18. Youngdahl, C. K. and Sternberg, E. "Transient Thermal Stresses in a Circular Cylinder." Jour. App. Mech., 84 (1961), 25.